THE ASTROPHYSICAL JOURNAL, 460:612–633, 1996 April 1

THE STATISTICS AND AGES OF COMPACT SYMMETRIC OBJECTS

A. C. S. READHEAD, G. B. TAYLOR, W. XU, AND T. J. PEARSON
California Institute of Technology, 105-24, Pasadena, CA 91125

AND

P. N. WILKINSON AND A. G. POLATIDIS
University of Manchester, Nuffield Radio Astronomy Laboratories, Jodrell Bank, Macclesfield, Cheshire SK11 9DL, England, UK
Received 1995 May 17; accepted 1995 October 3

ABSTRACT

Two dual frequency VLBI surveys of the compact structures in complete high-frequency samples of radio sources have been carried out. A classification of powerful extragalactic radio sources based on these surveys has revealed that $\sim 10\%$ of the objects are "compact symmetric objects" (CSOs) of an overall size $\lesssim 1$ kpc, with high-luminosity lobes straddling the center of activity. In many respects these objects mimic Cygnus A, but are smaller by a factor of 10^2–10^4. The working surfaces, or "hot spots," of the jets in CSOs are much closer to the central engine than in other powerful radio sources, and they provide both a new laboratory for the study of the physics of relativistic jets and a unique probe of the interstellar medium in the range 1–500 pc from the central engines of active galaxies.

The properties and statistics of CSOs are presented. The radio galaxy 2352+495 is shown to be a typical member of this class, and its optical and radio properties are discussed in detail. Our analysis of the hot spots in this object, in 0108+388, and in 0710+439 shows that if these are confined by ram pressure then CSOs have ages $\ll 10^6$ yr.

Two models for CSOs are investigated—a "fast" model in which the hot spots are advancing at $\sim 0.02c$ and a "slow" model in which the velocity of advance is $\sim 4 \times 10^{-3}c$. On the "slow" model, the morphology of these objects would be more spherical than is observed, and there would likely be more reddening of the narrow emission lines relative to the galactic continuum emission, whereas all of the observations are consistent with the fast model, in which the speed of advance is comparable to the speed of advance of the lobes in Cygnus A and the ages of CSOs are in the range 10^3–3×10^4 yr. This has interesting implications for their evolution which are discussed in a separate paper.

Subject headings: galaxies: active — galaxies: compact — galaxies: jets — radio continuum: galaxies — surveys

1. INTRODUCTION

One of the most significant results to emerge from studies of the radio morphology of active galactic nuclei, as revealed by ever more sophisticated observing and image reconstruction techniques over the last two decades, has been the near ubiquity of objects exhibiting an asymmetric one-sided nuclear jet, with no evidence of radio emission from the side opposite the jet on subkiloparsec scales, and the rarity of objects in which radio emission is seen on both sides of the central engine on scales of 1 pc–1 kpc (e.g., Readhead 1980; Zensus & Pearson 1987, 1990). In "compact symmetric objects" (CSOs), however, radio-emission regions *are* seen on both sides of the central engine on scales of 1 pc–1 kpc. We believe that CSOs may provide the key to the evolution of powerful extragalactic radio sources. The symmetry and the effects of relativistic beaming in CSOs have been discussed by Wilkinson et al. (1994), hereafter Paper I. The statistics and observed properties of CSOs are discussed in this paper (Paper II), and it is shown that, provided they are confined by ram pressure, these objects have ages $\ll 10^6$ yr, and it is argued that they have ages of 10^3–3×10^4 yr. The evolution of CSOs and of other classes of powerful extragalactic radio sources is discussed in a third paper (Readhead et al. 1996, hereafter Paper III).

A number of classes of powerful extragalactic radio sources have been recognized over the last three decades. On the large scale ($\gtrsim 15$ kpc), the most basic distinction is that between Fanaroff-Riley Class I (FR I) and Fanaroff-Riley Class II (FR II) objects (Fanaroff & Riley 1974, hereafter FR). On the small scale ($\lesssim 15$ kpc), the three major classes of object are the "compact flat spectrum" (CFS) objects (e.g., Readhead et al. 1978), the "compact steep spectrum" (CSS) objects (Peacock & Wall 1982; Fanti et al. 1990), and the "gigahertz-peaked spectrum" (GPS) sources (e.g., O'Dea, Baum, & Stanghellini 1991).

In order to explore the evolution of powerful extragalactic radio sources and to investigate the relationship between different types of radio-loud objects, we have undertaken a series of VLBI studies of complete samples to determine the compact structure. Three samples are being studied extensively by VLBI snapshot imaging—the sample of 65 objects with $S_{5\,\mathrm{GHz}} \geq 1.3$ Jy, $\delta > 35°$, $|b| > 10°$ (Pearson & Readhead 1988, hereafter PR); the first Caltech-Jodrell Bank sample (CJ1) of 135 objects with $1.3 > S_{5\,\mathrm{GHz}} \geq 0.7$ Jy, $\delta > 35°$, $|b| > 10°$ (Wilkinson et al. 1993; Polatidis et al. 1995; Thakkar et al. 1995; Xu et al. 1995); and the second Caltech-Jodrell Bank sample (CJ2) of 193 flat spectrum ($\alpha \leq -0.5$) objects with $0.7 > S_{5\,\mathrm{GHz}} \geq 0.35$ Jy, $\delta > 35°$, $|b| > 10°$ (Taylor et al. 1994; Henstock et al. 1995). All of the objects in these samples accessible to Mark II VLBI observations have been imaged with global VLBI arrays, and the PR and CJ1 samples are now well studied at both 1.6 and 5 GHz.

In the PR sample, there are a number of symmetric objects which have overall sizes of less than 1 kpc. They

appear to be similar in most respects, except size, to the radio doubles among the CSS objects in the complete low-frequency–selected sample studied by Fanti et al. (1985, 1990, 1995), which are typically a factor of ~ 10–100 larger than our objects. It seems most natural to explain the CSS radio doubles studied by the Fantis and their collaborators as the extension to larger physical size of the population of smaller symmetric objects that we have found in our high-frequency surveys. The symmetric objects that we have studied have much higher energy densities and pressures and much lower total energies than those of the larger CSS objects, and these characteristics enable us to place more stringent constraints on some of the alternative models for these objects.

To clarify the discussion we, in concert with Fanti et al. (1995), adopt the following terminology: "Compact symmetric objects" (CSOs) are those in which the separation between the symmetric lobes is less than 1 kpc, "medium-size symmetric objects" (MSOs) are compact steep spectrum doubles with lobe separations in the range 1–15 kpc, and "large symmetric objects" (LSOs) are objects with lobe separations greater than 15 kpc. These definitions are fairly arbitrary—at this point we attribute no physical significance to the size limits of the three classes. Throughout this paper we assume an Einstein–de Sitter universe with a Hubble constant $H_0 = 100\,h$ km s^{-1} Mpc^{-1}.

In this paper we first discuss CSOs and their statistics, and we show that the radio galaxy 2352+495 is a typical member of this class. We then analyze multifrequency VLBI observations of this object and determine the physical properties of the radio-emission regions. We show that it provides a useful probe of the interstellar medium on scales of 10–100 pc, and we use centimeter and millimeter radio observations of this object in conjunction with optical and X-ray observations to place interesting limits on the temperature and density of the confining medium in this region. We also discuss the age of CSOs and argue that they are young objects ($\sim 10^3$–10^4 yr), and are not old objects ($\sim 10^6$ yr) in which the expansion speed has been slowed to $\ll 0.02c$ by an unusually dense interstellar medium.

2. PROPERTIES AND STATISTICS OF CSOs

2.1. *Identification of CSOs*

The essential feature of CSOs is the high-luminosity radio components on both sides of the central engine on subkiloparsec scales. Throughout this paper we use the term "symmetric" to distinguish these objects from the majority of powerful extragalactic radio sources that show radio emission to only one side of the nucleus on subkiloparsec scales and are therefore "asymmetric." In Figure 1 we show images of five CSOs from the PR survey. Phillips & Mutel (1980, 1982) first drew attention to a class of objects which they interpreted as symmetric—there can be little doubt that their "compact double" sources (CDs) and our CSOs are the same types of object. However, although Phillips & Mutel interpreted the CDs as symmetric objects, they did not have compelling evidence of symmetry. The two components of CTD 93 are "leading edge" brightened (Mutel, Hodges, & Phillips 1985), and therefore this object looks symmetric and is almost certainly a CSO, but definitive proof of symmetry among CDs has been remarkably elusive, and it is now clear from multifrequency observations that some objects classified in the literature as CDs are not CSOs (Conway et al. 1994). In order to be sure that an object is symmetric, it is essential either that the center of activity be identified within the compact radio structure or that other compelling morphological evidence of symmetric structure be found, such as twin jets, twin hot spots, or relative motions indicative of symmetry (e.g., Taylor et al. 1996).

The demonstration of symmetry in these objects has proved to be crucial for progress in this field. The first observations of a CSO in which a component was seen between the two outer lobes were reported by Readhead, Pearson, & Unwin (1984), who drew attention to the radio galaxy 0710+439 ($z = 0.518$) as the most interesting structure that had been observed in the PR survey. Based on spectral index information, they correctly identified the southern end of the middle of the three components with the center of activity, and they concluded that the two outer components were regions of enhanced emission in two oppositely directed jets.

In an attempt to avoid proliferation of classes, Pearson & Readhead (1988) classified 0710+439 as a compact double object in spite of the fact that it had compact triple morphology, and for over a dozen years after making the first map of 0710+439, we classified these objects as compact doubles. However, this led to confusion when it became clear that there are compact double sources that are not CSOs (Conway et al. 1994), and we now believe that it is important to establish a classification that does not include physically distinct object types and which requires proof of symmetric ejection from the central engine for inclusion in the class.

Conway et al. (1992) discovered a second CSO—2352+495 ($z = 0.237$), the main subject of this paper—in the PR sample and used multiepoch data of both this object and 0710+439 to show that the flux densities of the middle components were varying with time, which was taken as further evidence that the center of activity in these objects is coincident with the middle component. Our first 1.6 GHz map of 2352+495 (Paper I) showed convincingly that the outer components are indeed lobes, and left no doubt that the center of activity lies between these components. We are now convinced, however, that although the center of activity lies close to the bright middle component, it is located not in the center but near the southern end of the middle component (see Fig. 1). In this regard it is remarkably similar to 0710+439. Conway et al. (1994) have argued that the object 0108+388 is also a CSO, and this interpretation has recently been confirmed with new observations at 8 GHz by Xu (1994) and at 15 GHz by Taylor et al. (1996).

Our determination of the location of the central engine in these three objects is derived from these 8 and 15 GHz VLBA maps. It is based on morphology, spectral index, and relative motions of the components in 0108+388; on morphology and relative motion of the components in 2352+495; and on morphology and spectral index of the components in 0710+439. A detailed discussion of the location of the centers of activity in these three CSOs is given by Taylor et al. (1996).

The objects 0108+388, 0710+439, and 2352+495 are our prime examples of the CSO class. They have symmetric hot spots, symmetric lobes, and a bright one-sided jet component, and any radio component coincident with the central engine is comparatively weak—typically only a few percent of the total flux density. In these three objects, the

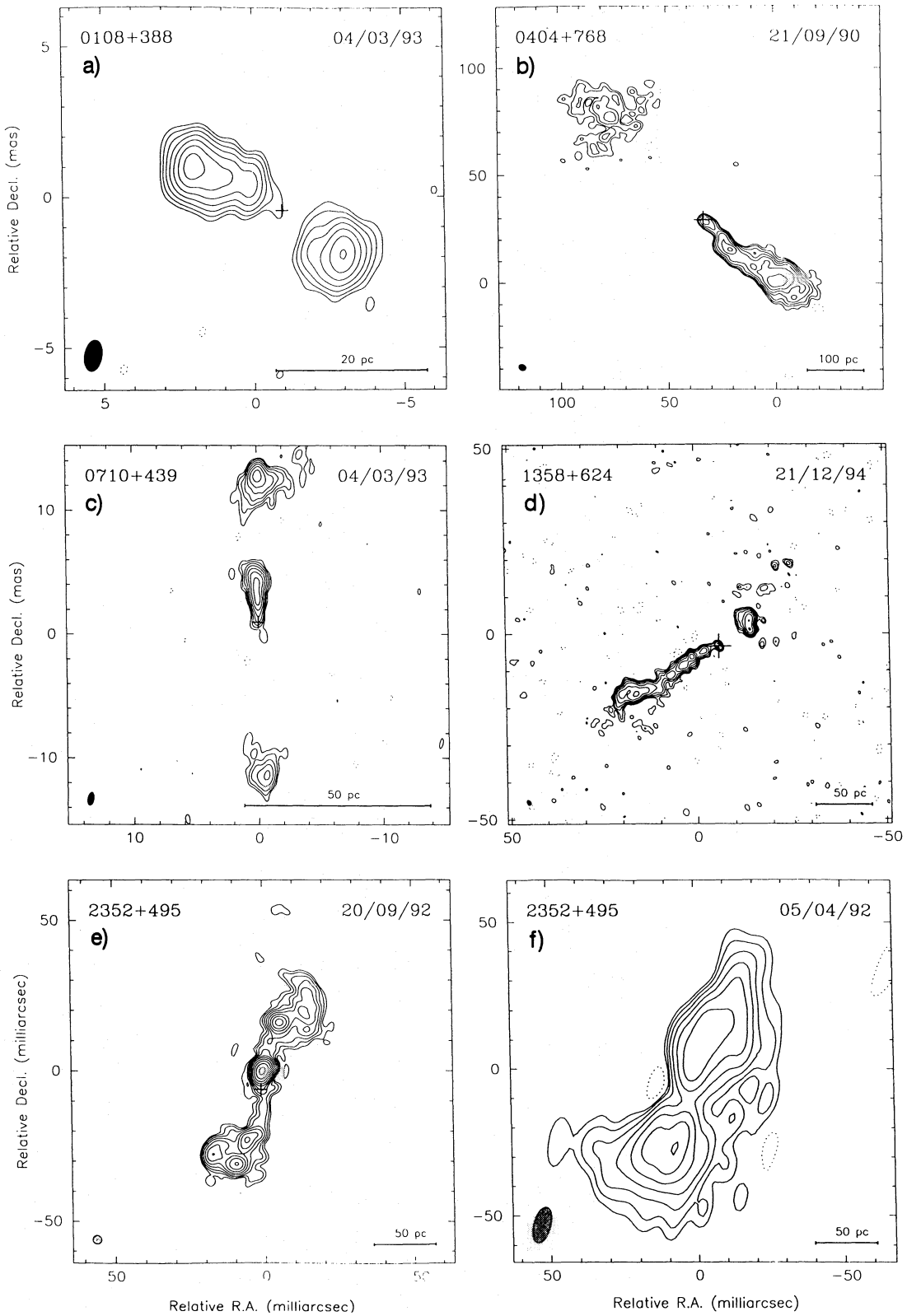

FIG. 1.—Maps of the five confirmed CSOs from the PR sample. (*a*) 0108+388 from 8.4 GHz observations of Xu (1994). (*b*) 0404+768 from 1.6 GHz observations of Polatidis et al. (1995). (*c*) 0710+439 from 8.4 GHz observations of Xu (1994). (*d*) 1358+624 from 8.4 GHz observations of Taylor et al. (1996). (*e*) 2352+495 from the full track 1.6 GHz observations reported in this paper. The observations were made with a 12-element global VLBI network over 12 hr. (*f*) Map of 2352+495 at 0.610 GHz made from the full track observations reported in this paper. The observations were made with a 10-element global VLBI network over 10 hr. The Mk II recording system was used for all observations, and the data were correlated on the JPL/Caltech Block II correlator. The maps were made with the Caltech "DIFMAP" package (Shepherd, Pearson, & Taylor 1994). In each map a cross marks the position of the radio core as determined from the source morphology, spectral indices, and/or component motions by Taylor et al. (1996). The contour levels, peak flux densities, and beam sizes are (*a*) – 1, 1, 2, 4, ..., 64% of 215 mJy beam^{-1}, 1.05 × 0.58 mas^2 in position angle (p.a.) – 10°2; (*b*) – 0.85, 1.7, 3.4, ..., 54% of 311 mJy beam^{-1}, 3.45 × 2.85 mas^2 in p.a. 75°0; (*c*) – 1, 1, 2, 4, ..., 64% of 160 mJy beam^{-1}, 1.06 × 0.50 mas^2 in p.a. – 9.8; (*d*) – 1, 1, 2, 4, ..., 64% of the peak (60 mJy beam^{-1}), 1.57 × 1.09 mas^2 in p.a. 33°6; (*e*) – 0.15, 0.15, 0.3, 0.6, ..., 77% of 818 mJy beam^{-1}, 3.00 × 3.00 mas^2; (*f*) – 1, 1, 2, 4, ..., 64% of 0.334 Jy beam^{-1}, 12.7 × 5.8 mas^2.

bright jet components are asymmetric, but, apart from this, there is no other asymmetric radio structure. There are four further possible CSOs in the PR sample—0404+768, 1031+567, 1358+624, and 2342+821. Multifrequency maps of these objects (Dallacasa et al. 1995; Pearson, Fassnacht, & Readhead 1996; Polatidis et al. 1995; Xu et al. 1995) show that 0404+768 and 1358+624 have symmetric lobes and asymmetric jets, but no clear hot spots. We classify them as CSOs because they have high-luminosity symmetric lobes—bringing the total of confirmed CSOs in the PR sample to five. It is possible that the radiation from the jets in these five objects is beamed. The case for including 1031+567 or 2342+821 in the CSO category is weaker than for the other candidates because we do not yet have the necessary high-quality images at enough frequencies to be sure that they are symmetric objects (Xu 1994), so we exclude them from the present discussion. Thus, there are five confirmed CSO and two candidates CSOs in the PR sample. In Table 1 we show the redshifts, luminosities, and lobe separations of the five confirmed CSOs in the PR sample.

The only quasar identified as a possible CSO in the PR survey is 2342+821. It is interesting that all five confirmed CSOs in the PR sample are galaxies, although we do have some CSO candidates that are quasars. It is clearly important to determine whether CSOs are predominantly galaxies. The galaxies that CSOs have been identified with are all elliptical galaxies, so that this raises, once again, the interesting question of why powerful radio sources are almost invariably associated with elliptical galaxies: what is it about elliptical galaxies that causes the central component to produce a radio source?

2.2. *Physical Properties of CSOs*

By definiton, CSOs have high-luminosity radio-emission regions on scales of 1 pc–1 kpc on both sides of the central engine, in contrast to one-sided core-jet objects in which radio emission is seen only on one side of the central engine on these scales. We do not require that CSOs are symmetric in *all* morphological features.

The five CSOs in the PR sample exhibit some or all of the following characteristics:

1. All of the CSOs that we have identified are high-luminosity objects. The monochromatic luminosity of 2352+495 is the lowest of the CSOs in the PR sample (see Table 1). By comparison, the boundary line in luminosity between FR I and FR II objects at 5 GHz, assuming a spectral index of −0.75, is more than a factor of 20 lower than the luminosity of 2352+495. Thus, by analogy with the large-scale counterparts, we designate the CSOs as "high-luminosity" objects, and for the purposes of this discussion we consider FR I objects to be "low-luminosity" objects.

2. The hot spots show no evidence of superluminal motion (0108+388, 0710+439, and 2352+495—Conway et al. 1992, 1994).

3. The jets are much brighter than the counterjets (all objects). The asymmetric jets seen in all five CSOs might be evidence for bulk relativistic motion.

4. The mean ratio of the two arm lengths for the PR CSOs is 1.2 ± 0.07, which gives a 3 σ upper limit of $0.3c$ on the velocity of advance of the jets.

5. The high-frequency spectra of CSOs are steep, with no hint of flattening with increasing frequency.

6. The parent objects are all elliptical galaxies—they all exhibit strong narrow emission lines in their spectra, but the continua are characteristic of an old stellar population. The luminosity is in the range $(0.3 \rightarrow 1)L^*$.

7. In the case of 2352+495, the isophotes are distorted, and there are nearby objects which might possibly be members of a cluster or evidence for interaction (O'Dea, Baum, & Morris 1990).

8. They exhibit weak radio variability—up to about 10% over periods of a few years (all objects), see PR.

9. They have low radio polarization—less than 0.5% at frequencies up to 5 GHz (all objects), see PR.

10. They have either no extended radio emission (all objects except 0108+388) or have very weak emission (0108+388).

11. They have very low core luminosities—typically less than a few percent of the total luminosity. This is the reason that CSOs have been so difficult to identify, and that the central components in CDs have been so elusive.

12. In a significant fraction of cases, they exhibit S-symmetry about the center of activity (0108+388, 0710+439, and 2352+495).

2.3. *Statistics of CSOs*

There are five CSOs and two CSO candidates in the PR survey out of a total of 65 objects. In the CJ1 survey there are 10 CSO candidates out of a total of 135, and in the CJ2 survey there are 22 candidates out of a total of 193. Thus, assuming a greater than 50% success rate in confirming CSOs, 5%–10% of the objects in complete flux density limited samples selected at 5 GHz are CSOs with separations less than 1 kpc. The numbers of CSOs, and of FR I, FR II, and D2 objects (Miley 1971), in the PR and CJ1 samples are given in Table 2.

It is important to consider whether we might have missed any CSOs in these surveys due to observational selection effects. We see from Table 2 that in the PR sample there are

TABLE 1

CSOs IN THE PR SAMPLE

Name	Redshift	m_v[a]	Radio Luminosity[b] (h^{-2} W Hz^{-1})	Lobe Separation (h^{-1} pc)
0108+388.....	0.699	22	9×10^{26}	25
0404+768.....	0.5985	22	1.2×10^{27}	450
0710+439.....	0.518	20.7	5×10^{26}	100
1358+624.....	0.431	20.9	4×10^{26}	120
2352+495.....	0.237	20.1	10^{26}	120

[a] All objects are elliptical galaxies.
[b] Evaluated at 5 GHz in the emitted frame.

TABLE 2

STATISTICS OF OBJECTS IN THE PR AND CJ1 SAMPLES

Sample	Optical Identification	CSO Candidate (<1 kpc)	Core jet or Complex (<1 kpc)	FR I (>1 kpc)	FR II (>1 kpc)	D2 (>1 kpc)	Unclassified (>1 kpc)	Total
PR	BL Lacs	0	1	0	1	5	2	9
	Galaxies	5	2	3	16	1	0	27
	Quasars	1	2	0	14	10	2	29
	Total	6	5	3	31	16[a]	4	65
CJ1.....	BL Lacs	0	1	0	2	4	2	9
	Galaxies	3	0	4	38	1	5	51
	Quasars	5	10	0	29	23	1	68
	Uncertain	2	1	0	2	2	0	7
	Total	10	12	4	71	30	8	135

[a] Includes 0108+388, which is a CSO with very faint extended structure.

seven galaxies with overall sizes less than 1 kpc, and five of these are CSOs or CSO candidates. The remaining two galaxies are M82 and 2021+614 (Conway et al. 1992). Thus, we have not missed any CSO galaxies in the PR sample—*all* galaxies with overall size less than 1 kpc are accounted for. The other PR CSO identified with a galaxy (0108+388) has faint extended structure and is therefore included under the D2 column in Table 2. There are 16 galaxies with overall sizes greater than 1 kpc in the PR sample.

In the CJ1 sample there are five galaxies and 15 quasars with overall sizes less than 1 kpc. Four of the galaxies and two of the quasars are CSO candidates. Thus, as in the case of the PR sample, almost all of the galaxies with overall sizes less than 1 kpc are CSOs or CSO candidates. The remaining objects in the CJ1 sample are all complex or core-jet objects. There are 37 FR II galaxies with overall sizes greater than 1 kpc in the CJ1 sample. Thus CSOs comprise $\gtrsim 50\%$ of the galaxies with overall extent less than 1 kpc in the PR and CJ1 surveys, and FR II galaxies outnumber CSOs by less than a factor of 10 in the PR and CJ1 surveys.

We conclude this section with a few comments on the surface brightness sensitivity of our 1.6 GHz observations. The relevant size range of extended jet/lobe components in a CSO at a typical moderate redshift is $\sim 10-\sim 100$ mas. Our simulations to test our surface brightness limits (Polatidis et al. 1995) show that with ≥ 12 antennas we would always detect 100 mas components with flux densities ≥ 300 mJy, and we would detect 10 mas components with flux densities ≥ 30 mJy. Thus we would detect CSO-size emission in a PR source as long as it contained more than 15% of the total flux density at 1.6 GHz at the upper end of the size range and more than 1.5% at the lower end of the size range. Our results show that we have detected extended emission on the 100 mas scale in a number of objects in the PR and CJ1 surveys, and the fact that we have not missed any CSOs due to surface brightness emission is borne out by the statistics of our complete samples, as shown at the beginning of this section.

In summary, we believe that we have detected all of the ~ 100 mas diffuse components in the complete CJ1 sample and in those PR objects which we have mapped at 1.6 GHz. There are 14 PR objects which we have not mapped at 1.6 GHz, but for these there are good quality maps in the literature. In a few of these cases, the maps do not rule out components of ~ 100 mas and more than 15% of the total flux density. We emphasize again, however, that these objects will not be galaxies with overall sizes less than 1 kpc, since all of these have been accounted for, as shown above.

3. RADIO PROPERTIES OF 2352+495

In view of the fact that 2352+495 exhibits all of the properties 1–12 of § 2.2, it is reasonable to consider this object as an archetype of the CSO class. The properties of 2352+495 which we deduce in the following sections are typical of CSOs in the PR sample.

We have made VLBI observations of 2352+495 at 610 MHz and 1.66 GHz. The maps from these observations are shown in Figures 1*e* and 1*f*. The 1.66 GHz image shows the structure most clearly and leaves no doubt that this is indeed a "symmetric" object. Previous observations at 5 and 10.7 GHz have been reported by Conway et al. (1992), and first-epoch (snapshot) observations at 1.66 GHz have been described in Paper I. We have combined the 5 and 10.7 GHz observations with the observations at 610 MHz and 1.66 GHz to identify the principal components of the object and to determine the angular sizes and the flux densities of these components.

Our new observations at 1.66 GHz (Fig. 1*e*) are more sensitive than our previous snapshot observations (Paper I), and they show clearly that 2352+495 has twin jets. Given the location of the center of activity, marked with a cross in Figure 1*e*, we see that there is a bright feature in the northern jet, which we refer to as the "bright jet feature." Note that the primary (northern) jet is considerably brighter than the counterjet. The combination of these observations and those at 610 MHz and 5 GHz shows that we are seeing symmetric hot spots and outer lobes. It is clear, therefore, that CSOs are morphologically very similar to larger scale objects classified as FR II objects. The arguments are compelling that the lobe and hot spot emission in CSOs is fairly isotropic (Paper I), which is important for determining the physical properties in these radio-emission regions.

3.1. *Flux Densities, Spectra, and Angular Sizes of Radio Components*

We have identified the major features of 2352+495 as follows—the 5 and 10.7 GHz maps of Conway et al. (1992) are most useful in delineating high surface brightness flatter spectrum components. These indicate clearly the bright jet component and two "hot spots" which straddle the center of activity. From the 1.66 GHz image of Figure 1*e*, we see

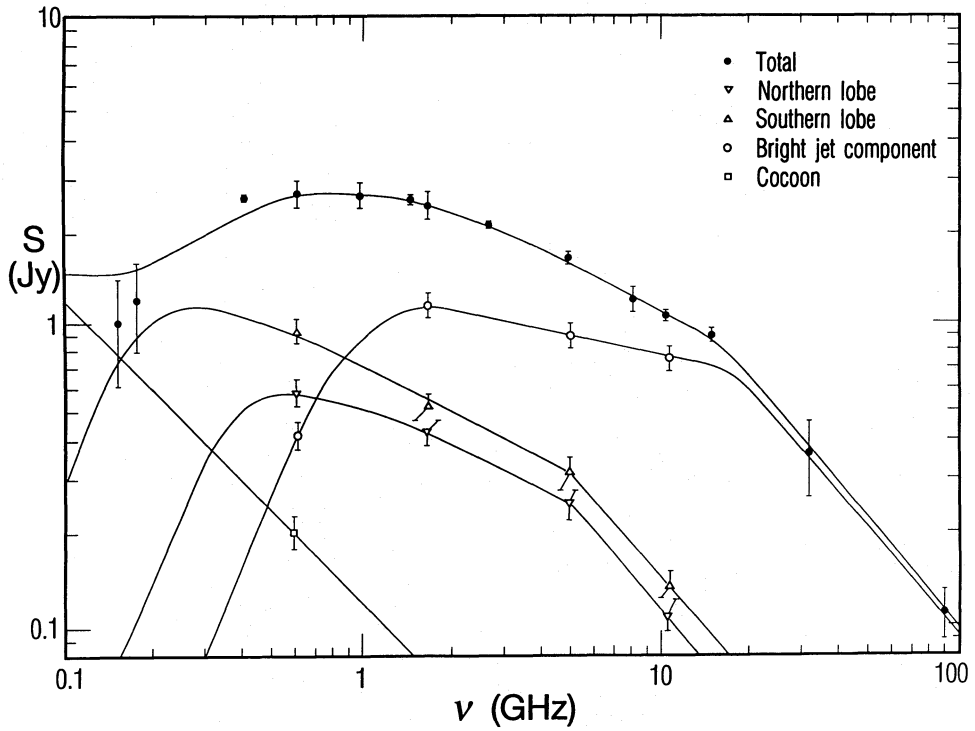

FIG. 2.—Radio spectrum of 2352+495. The upper curve shows the total spectrum of 2352+495. Also shown are the spectra of the northern and southern lobes and the spectrum of the bright jet feature.

that the hot spots are embedded in lower surface brightness features, which we identify with "lobes." The jets are most clearly visible in this figure, as are the higher surface brightness portions of the lobes, but the full extent of the lobes is most clearly visible in the 610 MHz image shown in Figure 1*f*.

The total spectrum and the spectra of the individual components are shown in Figure 2. The flux densities, spectral indices, and angular sizes of the various components are given in Tables 3, 4, and 5. Wherever possible, we use flux densities and angular sizes derived from least-squares fitting of Gaussian components to the visibility data, since these are more accurate than flux densities measured directly from maps.

All angular sizes measured from maps or derived from models are FWHM. The angular sizes of the components of 2352+495 (Table 5) are derived from a combination of the images shown in Figures 1*e* and 1*f*, and of models of the major components. The bright jet component (B_1 and B_2) and hot-spot angular sizes we adopt are taken directly from the model fits given in Table 5 of Conway et al. (1992). We have increased these by a factor of 1.8 in order to allow for the fact that these are FWHM of Gaussian distributions, whereas our calculations use the diameter of a uniform spherical source.

3.1.1. *The Lobes*

The surface brightness of the lobes is too low to measure their flux densities at 5 and 10.65 GHz. However, it is possible to make a reasonable estimate as follows: The ratio of

TABLE 3

FLUX DENSITIES OF COMPONENTS OF 2352+495 (Jy)

Component	610 MHz[a]	1.66 GHz[a]	5 GHz	10.65 GHz
Northern hot spot	0.17	0.18	0.08[b]	0.03[c]
Southern hot spot	0.15	0.14	0.04[b]	0.02[c]
Northern jet	0.13	0.033	...	...
Southern jet	0.02	0.03	...	...
Northern lobe	0.59	0.43	0.26[h]	0.11[h]
Southern lobe	0.93	0.52	0.32[i]	0.13[i]
Bright jet component	0.42	1.15	0.91[d]	0.76[e]
Combined lobes (northern & southern)	1.52	0.95	0.58[f]	0.24[f]
Cocoon	0.20	...	...	...
Total flux density	2.61	2.50	1.60[g]	1.05[g]

[a] Images shown in Figures 1*e* and 1*f*.
[b] Table 5, Conway et al. 1992.
[c] Table 6, Conway et al. 1992.
[d] Table 5, Conway et al. 1992, components $B_1 + B_2$.
[e] Table 5, Conway et al. 1992, components $B_{1A} + B_{1B} + B_2$.
[f] Total flux density minus northern and southern hot spots and bright jet component.
[g] Data used in Fig. 3 of Conway et al. 1992.
[h] 0.45 times combined lobes, see text.
[i] 0.55 times combined lobes, see text.

TABLE 4

SPECTRAL INDICES OF COMPONENTS OF 2352+495

Component	610 MHz–1.66 GHz	1.66 –5 GHz	5–10.65 GHz
Northern lobe	−0.30	−0.5	−1.1
Southern lobe	−0.50	−0.5	−1.1
Middle component.....	+1.0	−0.25	−0.25
Cocoon[a].....	−1.0	−1.0	−1.0

[a] We assume a spectral index of −1.0 for the cocoon, see text.

the flux densities of the northern to southern lobe is 0.64 at 610 MHz and 0.82 at 1.66 GHz. It appears that both lobes are synchrotron self-absorbed at low frequencies (see § 3.2). We therefore ascribe the change in the flux-density ratio of these two components between 1.66 GHz and 610 MHz to synchrotron self-absorption and take the value at 1.66 GHz to be the true optically thin flux-density ratio of these two regions (0.82). We then assume that the ratio of the northern to southern component flux densities is 0.82 at both 5 and 10.65 GHz. We estimate the flux density in the two lobes combined by subtracting the flux densities of the bright jet components and the hot spots from the total flux density. Note that the flux densities of the hot spots are much smaller than those of the lobes, so that any uncertainties in the flux density of the hot spots do not greatly affect this result.

We are confident of the derived spectral indices for the lobes, because these features contribute a large fraction of the total flux density at all frequencies we have observed.

3.1.2. *The Cocoon*

The total flux density of 2352+495 is well accounted for in our images. At 610 MHz, ~0.2 Jy is seen in diffuse emission around the lobes. We ascribe this emission to a cocoon. We have made a spectral index map (not shown) between 610 MHz and 1.66 GHz, which shows that the cocoon has a steep spectrum, with $\alpha_{0.610}^{1.66} \sim -1$. Apart from the cocoon, there is no evidence for any halo or larger radio structure. We have made observations with MERLIN at 408 MHz that enable us to place a limit of 50 mJy on any structure on scales of 0.″1–4″. The angular size of the cocoon has been determined from the overall extent of the source, which is ~90 × 25 mas. We assume that the cocoon is a prolate spheroid, and therefore we use an angular size of $(90 \times 25 \times 25)^{1/3}$ mas, i.e., 35 mas, to characterize the size of the cocoon.

3.2. *Interpretation of the Radio Spectra*

We now discuss the main features of the total spectrum and of the spectra of the lobes of 2352+495 shown in Figure 2. An obvious feature in the total spectrum is the low-frequency cutoff, which is almost certainly due to synchrotron self-absorption. But we do have to consider the alternative explanation of free-free absorption, which has been suggested as an explanation for the cutoff in GPS and many CSS objects (van Breugel 1984; O'Dea et al. 1991).

3.2.1. *Free-Free Absorption*

The total spectrum between 2.7 and 15 GHz is well fitted by a power law with slope $\alpha = -0.50$. Extrapolating this spectrum down to 151 MHz yields a flux density at this frequency of 9 Jy, whereas the observed flux density at 151 MHz is 1.0 ± 0.4 Jy. If the low-frequency cutoff were due to free-free absorption, the optical depth at 151 MHz would be $1.8 < \tau_{0.151} < 2.7$, and that at 610 MHz would be $\tau_{0.610} = 0.6$. These values are inconsistent with the expected behavior $\tau \propto \nu^{-2.1}$ for free-free absorption. As discussed in the following section, unless the lobes are extremely far from equipartition, they must be synchrotron self-absorbed at frequencies below ~500 MHz. We therefore conclude that the low-frequency cutoff is due not to free-free absorption but to synchrotron self-absorption. We have fitted synchrotron self-absorption spectra for a homogeneous source to the component spectra (see Fig. 2), and hence we derive a more stringent upper limit on the optical depth at 151 MHz due to free-free absorption of $\tau_{0.151} < 1$.

3.2.2. *Synchrotron Self-Absorption*

Synchrotron self-absorption may be discussed in terms of the "equipartition brightness temperature" (Readhead 1994). From Figure 2 we see that the northern and southern lobes have peak flux densities of 0.6 Jy at 600 MHz and 1.0 Jy at 400 MHz. For a spectral index in the optically thin

TABLE 5

ANGULAR SIZES[a] OF COMPONENTS OF 2352+495

Component	Major Axis (Gaussian Model) (FWHM)	Minor Axis (Gaussian Model) (FWHM)	Size[b] (Spherical Model)
Northern hot spot	0.81	0.46	1.1
Southern hot spot	1.51	1.35	2.6
Northern lobe	...	...	10
Southern lobe	...	...	15
Middle component B_1.....	1.15	1.02	1.95
Middle component B_2.....	1.07	0.46	1.25
Cocoon[b]	...	...	35

[a] All values are milliarcseconds.
[b] See text.

regime in the range -0.5 to -0.75, this yields equipartition brightness temperatures for both lobes of $\sim 7 \times 10^{10}$ K. The equipartition brightness temperature is weakly dependent on observable quantities (Readhead 1994). The observed peak brightness temperatures are 3×10^{10} K and 5×10^{10} K for the northern and southern lobes, respectively. Given the uncertainties in the observations, the observed peak brightness temperatures are consistent with the equipartition values. Note that the "equipartition Doppler factor" (Readhead 1994) is in the range 0.5–1 in both lobes—in agreement with the conclusion of Paper I that relativistic beaming effects are small in the lobes.

The fact that the spectrum of the higher surface brightness lobe cuts off at a higher frequency and that synchrotron self-absorption must occur in these components at close to the observed turnover frequencies unless they are extremely far from equipartition (Readhead 1994) leads us to conclude that the low-frequency turnover is due to synchrotron self-absorption not to free-free absorption.

Between 1.66 and 5 GHz, the spectra of the lobes should be free of any effects due to synchrotron self-absorption. We have already ruled out the possibility of free-free absorption above 1 GHz, therefore we conclude that the spectrum of the lobes between 1.66 and 5 GHz is the undistorted optically thin spectrum. The optically thin spectral index in these components is therefore $\alpha = -0.5$ (see Table 4). We use this value for the remainder of the discussion.

3.2.3. *The High-Frequency Break in the Lobe Spectra*

It can be seen in Figure 2 and in Table 4 that there is a break in the spectrum of the lobes at high frequencies—from $\alpha_{1.66}^{5} = -0.5$ to $\alpha_{5}^{10.65} = -1.1$. Note that the results for the northern and southern lobes are not independent, because of our assumption that the flux-density ratio in these two components is constant in the optically thin regime (see § 3.1). There is a clear break in the spectrum at ~ 5 GHz, with $\Delta\alpha \approx -0.5$. We therefore attribute the change in spectral index at 5 GHz to synchrotron losses (e.g., Leahy 1991).

3.3. *Physical Properties of the Radio Components*

The linear sizes, brightness temperatures (T_b), equipartition magnetic fields (B_{eq}), minimum energies, bolometric luminosities (L), and synchrotron lifetimes of the different components we have identified in 2352+495 are given in Table 6. In all of our calculations we assume an electron-positron plasma ($k = 0$), a "tangled" magnetic field, and equipartition between the magnetic field and the particles, i.e., $u_B = u_{rel}$. For the case of an electron-proton plasma with equal energy densities in protons and electrons ($k = 1$), the protons are not relativistic and $u_{proton} = u_{rel}$, equipartition gives $u_B = 2 \times u_{rel}$, and, assuming pressure $p = (2 \times u_{rel} + u_B)/3$, densities and masses based on ram pressure will be a factor of 2 greater than those given below.

We also assume an optically thin spectral index of -0.5 for all components except the cocoon ($\alpha = -1.0$), and we assume lower and upper cutoffs of the electron energy distribution corresponding to radiation at 10^7 and 10^{11} Hz in the emission rest frame, respectively. For $\alpha \sim -0.5$, a change in the upper or lower cutoff by a factor of 10 causes a change of $\sim 15\%$ in the calculated minimum energy, while changes in the upper cutoff by an order of magnitude cause changes of a factor ~ 3 in the bolometric luminosities, and changes in the lower cutoff by an order of magnitude cause $\lesssim 2\%$ changes in these luminosities. These effects should be borne in mind in the discussions of §§ 5–9.

4. OBSERVATIONS OF 2352+495 IN OTHER WAVE BANDS

4.1. *Infrared Observations*

The 60 μm *IRAS* flux density of 2352+495 is less than 90 mJy (3 σ upper limit), and, similarly, in the other PR CSOs the infrared luminosity is below the *IRAS* sensitivity limit. There is no evidence, therefore, of infrared emission from CSOs. The limit on the infrared luminosity in 2352+495 at 60 μm is a factor of 6 below that of Arp 220 (at the relevant frequency). It is clear that CSOs are significantly less luminous than hyperluminous infrared galaxies (e.g., Cutri et al. 1994).

4.2. *Optical Observations*

High-quality 200 inch telescope optical spectra have been obtained for all the objects in the PR sample (Lawrence et al. 1996). These show that the spectra of the PR CSOs are all rather similar, and that the spectrum of 2352+495, shown in Figure 3, displays properties seen in the spectra of most other members of this class—one object (0404+768) shows considerably more reddening in the narrow lines. The host galaxy of 2352+495 has $z = 0.237$ and has the following characteristics (see Fig. 3 and Table 7):

1. It has a fairly red continuum spectrum with overall shape typical of an old stellar population, with molecular

TABLE 6

PHYSICAL PARAMETERS[a] OF COMPONENTS OF 2352+495

Component	Size (h^{-1} pc)	T_b[b] (K)	B_{eq} ($h^{2/7}$ G)	u_{min}[c] ($h^{4/7}$ ergs cm^{-3})	U_{min}[c] ($h^{-17/7}$ ergs)	L (h^{-2} ergs s^{-1})	τ_{synch}[d] ($h^{-3/7}$ yr)
Northern hot spot	3	5×10^{10}	3×10^{-2}	6×10^{-5}	1.5×10^{52}	2×10^{42}	100
Southern hot spot	6	3×10^{10}	10^{-2}	10^{-5}	3×10^{52}	10^{42}	500
Northern lobe	25	3×10^{10}	6×10^{-3}	3×10^{-6}	5×10^{53}	8×10^{42}	1200
Southern lobe	35	7×10^{10}	4×10^{-3}	1.5×10^{-6}	10^{54}	10^{43}	1800
Bright jet component B_1	5	2×10^{10}	3×10^{-2}	7×10^{-5}	10^{53}	2×10^{43}	100
Bright jet component B_2	3	2×10^{11}	4×10^{-2}	10^{-4}	4×10^{52}	10^{43}	80
Cocoon	85	3×10^{10}	1.5×10^{-3}	2×10^{-7}	2×10^{54}	10^{42}	7500

[a] For $H_0 = 100\,h$ km s^{-1} Mpc^{-1}, and $q_0 = 1/2$.

[b] T_b is at 2 and 1 GHz for the northern and southern hot spots, respectively; at 0.3 and 0.55 GHz for the northern and southern lobes, respectively; at 3 and 2 GHz for B_1 and B_2, respectively; and at 151 MHz for the cocoon.

[c] The minimum energy density given above is $u_{min} = u_{rel} + u_B$. Likewise, the minimum energy is $U_{min} = U_{rel} + U_B$. The pressure in an electron-positron plasma is assumed to be $p = u_{min}/3$.

[d] Synchrotron-loss timescales are given for a spectral break at 5 GHz for the lobes and 15 GHz for the bright jet components (see text).

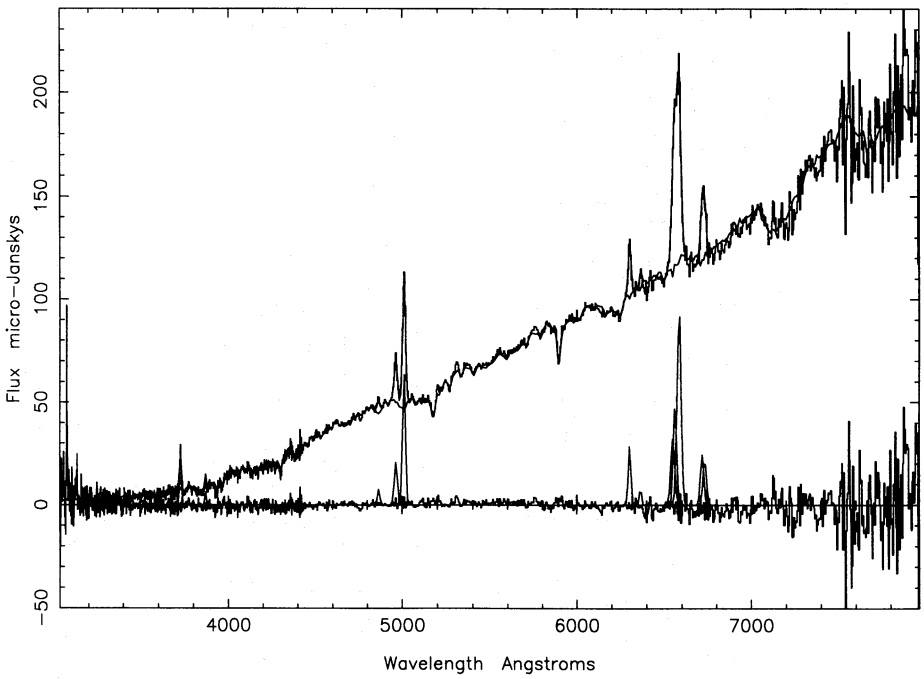

FIG. 3.—Optical spectrum of 2352+495. This spectrum from the Palomar 200 inch telescope shows many features which are typical of active elliptical galaxies and of CSOs. It has been fitted with a template spectrum constructed from local elliptical galaxies which has been dereddened by $E_{B-V} = 0.13$ (see text). The upper plot shows the calibrated spectrum with elliptical galaxy template superposed. In the lower plot, the template has been subtracted from the spectrum to show the fitted emission lines (Lawrence et al. 1996). We see a strong 4000 Å break, molecular absorption bands, and a fairly red continuum—all of which indicate an old stellar population. The Balmer decrement indicates modest reddening of the lines $E_{B-V} = 0.30$, i.e., significantly greater than the reddening of the continuum.

absorption lines which are seen in old stars. The continuum is well fitted by a template spectrum made up from spectra of low-redshift elliptical galaxies (Lawrence et al. 1995) and with reddening $E_{B-V} = 0.13$. We note that the spectrum of 2352+495 is very difficult from the spectra of typical starburst galaxies (e.g., Osterbrock 1987), since it does not show a strong blue continuum or Balmer absorption lines.

2. The spectrum displays narrow permitted and forbidden lines. The relative line strengths are typical of radio galaxies. For comparison, these are also given for Cygnus A (Osterbrock 1989). Both objects satisfy the LINER requirements suggested by Osterbrock (1989), except in the [O III]/Hβ ratio.

3. It shows a 4000 Å break, which is typical of galaxies dominated by an old stellar population, and is not seen in starburst galaxies (although this break is seen in post-starburst galaxies).

The galaxy has $m_v = 20.1$ (Fanaroff & Blake 1972), thus, after correcting for reddening and applying the K-correction for an object at a redshift of 0.237, we find $M_V = -19.8$. From our spectrum we see that 2352+495 is 1.3 mag fainter in the B band, and hence $M_B = -18.6$—where we have also corrected for the small difference in reddening between the B and V bands. We compare this with the value obtained by Efstathiou, Ellis, & Peterson (1988) of $M_{B_T} = -19.7$, and hence we find that the optical luminosity of

TABLE 7

EMISSION-LINE STRENGTHS AND WIDTHS IN 2352+495

Line	Line Strength[a] (ergs s^{-1})	Line Width (FWHM) (Å)	Line Strength Relative to Hβ	Cygnus A Line Strength Relative to Hβ[b]
[O II]3726,3729.....	1.88E+41	9.4	4.46	5.00
[Ne III]3868.76	2.72E+40	6.3	0.65	1.23
Hβ 4861	4.21E+40	16.7	1.00	1.00
[O III] 4959	1.40E+41	21.5	3.32	3.88
[O III] 5007	3.94E+41	20.1	9.35	12.30
[O I] 6300	7.24E+40	17.3	1.72	1.10
[O I] 6364	1.70E+40	11.2	0.40	0.35
[N II] 6548.....	1.06E+41	26.1	2.52	1.90
Hα 6563	1.31E+41	20.7	3.10	3.08
[N II] 6583.....	3.10E+41	26.2	7.36	6.15
[S II] 6716	6.41E+40	22.9	1.52	1.66
[S II] 6731	5.98E+40	23.0	1.42	1.51

[a] All line strengths have been corrected for reddening assuming case B recombination and a Balmer decrement of 3.1, which yields ($E_{B-V} \approx 0.30$).

[b] From Osterbrock 1987.

2352+495 is $\sim 0.35 L_*$. For comparison, typical large FR II objects are associated with elliptical galaxies with $L \sim L_*$ (Owen & White 1991).

The relative line strengths are rather similar to those in Cygnus A, which we regard as good evidence that the excitation mechanism is photoionization (e.g., Osterbrock 1987). We assume case B recombination with a Balmer decrement of 3.1 and, hence, derive extinction of $E_{B-V} = 0.30$. With this reddening, we derive the dereddened line strengths given in Table 7. The total narrow line luminosity of 2352+495 is $1.1 \times 10^{42} h^{-2}$ ergs s^{-1}.

We assume that the temperature of the narrow emission-line regions is in the range 10^4 to 2×10^4 K. The ratio of the [S II] $\lambda\lambda$6716, 6731 lines then implies that $N_e \sim 600$ cm^{-3} for $T \sim 10^4$ K and $N_e \sim 850$ cm^{-3} for $T \sim 2 \times 10^4$ K, so that the pressure in the narrow emission-line regions is $1\text{–}2 \times 10^{-9}$ dyn cm^{-2}, i.e., much lower than the pressures in the hot spots, lobes, or even the cocoon of the radio source. A typical velocity dispersion is that of the [O III] $\lambda\lambda$4959, 5507 lines, which both have FWHM = 700 km s^{-1}.

We estimate the mass of the narrow emission-line regions from the (corrected) Hβ line luminosity to be $(2\text{–}4) \times 10^8 N_e^{-1} M_\odot$ for $T \sim (1\text{–}2) \times 10^4$ K. If this material were uniformly distributed in a spherical cloud, the radius of the cloud would be ~ 13 pc. However, if the narrow emission-line clouds in 2352+495 are like those in other radio galaxies, then they are spread out over a region a few hundred parsecs in radius. In this case the filling factor is only $\sim 10^{-6}$, so that the material responsible for the narrow line emission is very clumpy.

Stanghellini et al. (1993) have made $r - i$ observations of a number of galaxies. Eight of these have known redshifts and are discussed by O'Dea et al. (1994a, see also O'Dea et al. 1992). They find five galaxies with $r - i$ colors which are typical of elliptical galaxies. However, three objects have $r - i$ colors 1–2 mag larger than typical elliptical galaxies. These three objects are 0108+388, 0404+768, and 0710+439, i.e., they are all CSOs. Thus, there is some evidence for a significant difference in color between some CSOs and typical elliptical galaxies. One CSO observed by Stanghellini et al. (1993)—1358+624—has typical elliptical galaxy $r - i$ color. In addition, one of us (G. B. T.) has measured the $r - i$ color of 0710+439 to be 0.76 ± 0.05, which is 1.1 mag lower than the value reported by Stanghellini et al. (1993), i.e., it too has typical elliptical galaxy $r - i$ color. Except for 0404+768, the extinctions in the narrow emission-line regions are small. It is possible that the very red $r - i$ colors in 0108+388 and 0404+768 are due to the presence of a very red compact nuclear source. Evidence that 0108+388 has a very red nuclear source is presented by O'Dea et al. (1992). This interpretation is consistent with our finding above for 2352+495 that the narrow line emission is significantly more reddened than the stellar emission.

4.3. *X-Ray Observations*

O'Dea et al. (1994b) made *ROSAT* observations of 2352+495 to look for evidence of a cluster. They did not detect the object and placed a 3 σ upper limit on the X-ray luminosity in the 0.2–2.0 keV band of less than $1.7 \times 10^{42} h^{-2}$ ergs s^{-1} for both a point source and an extended (200 kpc radius) source. O'Dea et al. (1995) corrected this for absorption in our Galaxy, and they derive a maximum permitted luminosity at the 3 σ level of less than $3.4 \times 10^{42} h^{-2}$ ergs s^{-1}. If 2352+495 is typical of CSOs in X-ray emission (as it is in most other properties observed thus far), then these objects are not strong X-ray emitters, and they reside in poor clusters or in small groups of galaxies. The X-ray luminosity limit is low for an average FR II object but consistent with the level of X-ray emission seen in FR I objects (Fabbiano et al. 1984).

We have calculated the expected X-ray luminosities of the bright jet components due to inverse Compton scattering. We find that the luminosity for the component which has its peak flux density at 2 GHz, whether it be B1 or B2, is just consistent with the upper limit measured by O'Dea et al. (1995), while that for the other component is well below this limit. Thus, more sensitive X-ray observations might well provide a measure of the Doppler boosting (if any) in one of the bright jet components.

5. THE JETS IN 2352+495

We now consider the physical properties of the jets in 2352+495. We have seen in § 4.2 that the pressure in the optical emission-line regions is 4 orders of magnitude lower than the pressure in the hot spots. Therefore, if the pressure in the interstellar medium between the narrow line clouds is comparable to the pressure in the clouds, then either the hot spots must be confined by ram pressure interaction with the interstellar medium or they must be magnetically confined. We assume that they are confined by ram pressure.

5.1. *Bulk Velocity and Power*

In the nonrelativistic case, and assuming steady flow, the jet power is $Q_j = \rho_j v_j A_j(\frac{1}{2}v_j^2 + w_j)$, and the momentum flux, i.e., the thrust or force of the jet, is $F_j = A_j(\rho_j v_j^2 + p_j)$, where ρ_j, v_j, A_j, p_j, and w_j are, respectively, the density, velocity, cross-sectional area, pressure, and enthalpy of the jet (Landau & Lifshitz 1959). For the case of a highly relativistic jet, with equation of state $p \propto \rho^{4/3}$, the jet power and thrust are given by $Q_j = 4p_j\gamma_j^2 v_j A_j$ and $F_j = (4\gamma_j^2\beta_j^2 + 1)p_j A_j$, where γ_j is the jet Lorentz factor and $\beta_j = v_j/c$ (Landau & Lifshitz 1959; Blandford 1990). Hence we may express the relationship between the jet power and the jet thrust in the form

$$Q_j = \Phi v_j F_j , \tag{1}$$

where $\Phi = (5\mathcal{M}^2 + 15)/(10\mathcal{M}^2 + 6)$ for a supersonic, nonrelativistic jet with specific-heat ratio 5/3, $\mathcal{M}$ being the Mach number; and $\Phi = 4/(1 + 3\beta_j^2)$ for a highly relativistic jet.

We consider the situation in a steady jet, which we assume to be supersonic (e.g., Blandford & Rees 1974) and in which the hot spot is moving forward at a steady velocity of advance, v_a. We assume pressure p in the hot spot, and we consider the forces at two interfaces—first, the interface between the hot spot and the jet and, second, the interface between the hot spot and the shocked interstellar medium. In practice, these are complex interfaces (e.g., Lind et al. 1989), but these details do not affect the following simple calculations. At the first interface the hot spot pressure forces must balance the thrust of the jet, since the hot spot is not accelerating, i.e., $F_j = pA$, where A is the cross-sectional area of the hot spot. Thus we have from equation (1),

$$Q_j = \pi r^2 p \Phi v_j , \tag{2}$$

where r is the radius of the hot spot, here assumed equal to

the radius of the jet. The input jet power is equal to the sum of the power expended against the external medium in advancing the hot spot (Q_a), the bolometric radio luminosity of the hot spot (L_h), and the power injected into relativistic particles and magnetic field in the lobes (Q_l) and cocoon ($Q_c/2$):

$$Q_j = Q_a + L_h + Q_l + Q_c/2 \,. \tag{3}$$

In the case of a nonrelativistic supersonic jet, the range of $\mathcal{M}$ ($\mathcal{M} = 1 \rightarrow \gg 1$) yields $\frac{1}{2} \leq \Phi \leq \frac{5}{4}$. A lower limit on the jet power is given by the bolometric radio luminosities of the hot spot, lobe, and cocoon, since $Q_j \geq L_h + L_l + L_c/2$. Hence, using the upper limit on Φ and applying equation (2), we have

$$v_j \geq \left(\frac{1}{\pi r^2 p 5/4}\right)(L_h + L_l + L_c/2) \,. \tag{4}$$

Thus, using the values of these parameters given in Table 6, and excluding the bright jet component, since this may be relativistically beamed, we determine the lower limits on jet velocities given in Table 8. We see that the jet velocities in 2352+495 are $\gtrsim 0.3c$. This is the first instance in which it has been possible to use hot spots to determine a lower limit on the jet velocity of a parsec-scale jet. Note that $\gamma_j \approx 1.05$ for $v_j \approx 0.3c$, so that the nonrelativistic formulation is appropriate in determining this lower limit.

We now estimate the power supplied by the jet by placing lower and upper limits on it. As we have seen, the luminosity of the hot spot, lobe, and cocoon provides a firm lower limit to Q_j. The maximum value of the product Φv_j is $2c/3^{1/2}$, so

$$Q_j \leq \pi r^2 p 2c/\sqrt{3} \,. \tag{5}$$

Hence, from equations (4) and (5), and with the values given in Table 6, we find that

$$10^{43}\ h^{-2}\ \text{ergs s}^{-1} \leq Q_j \leq 3.2 \times 10^{43}\ h^{-10/7}\ \text{ergs s}^{-1} \,,$$

where we have taken the mean of the values for the two jets. Note that we can determine the jet power to within a factor of 3. The limits derived for the northern and southern jets agree to within $\approx 10\%$, and if the bulk velocity is the same in the two jets, the jet powers agree equally well. The lower limit is very conservative, so we will assume that $Q_{j,n}$ and $Q_{j,s}$ are both $\sim 3 \times 10^{43}\ h^{-10/7}$ ergs s^{-1} (we designate the northern and southern features by the subscripts n and s). We note that the uncertainties in the upper and lower cutoffs in the electron energy distribution (§ 3.3) have little effect on the upper limit to Q_j but have an appreciable effect on the lower limit—a change of a factor of 10 in the upper cutoff gives a change of a factor of 3 in the lower limit to Q_j.

We assume that the hot spot is confined by ram pressure with the interstellar medium, so that at the second interface

$$p = \rho_{\text{ext}}\, v_a^2 \,, \tag{6}$$

where ρ_{ext} is the density in the interstellar medium and v_a is the velocity of advance of the jet. The thrust, F, of each jet is also given in Table 8. In the case of equipartition, $F \propto S^{4/7} r^{2/7}$, where S is the flux density of the hot spot, so that the thrust can be determined rather accurately from the observations. We assume that the uncertainties in the flux density, angular size, and distance from the core of the hot spot are 10%, 10%, and 5%, respectively, and hence determine the uncertainties in the thrusts given in Table 8. Notice that the thrusts of the two jets in 2352+495 agree within the (small) uncertainties.

The work done by the hot spot in advancing through the interstellar medium a distance d is $W_a = Fd$. We assume that the thrust is constant so that, since d can be measured accurately, it is possible to determine W_a accurately for an assumed value of H_0. The power required for this advance is $Q_a = W_a/\tau_j$, where τ_j is the age of the jet. Hence we derive the values for $W_{a,n}$ and $W_{a,s}$ given in Table 8. In Table 8 we also give the powers consumed in the advance of the two jets, $Q_{a,n}$ and $Q_{a,s}$, and in supplying the lobe energy, $Q_{l,n}$ and $Q_{l,s}$. In calculating Q_l, we assume a straight spectrum up to our upper cutoff of 10^{11} Hz, since we are interested in the total power injected into the lobe, i.e., before synchrotron losses. We see in Table 8 that, if $\tau_j \sim 3000$ yr, Q_a and Q_l are comparable to L_l, whereas, if $\tau_j \gg 3000$ yr, they are negligible compared with L_l.

5.2. "*Waste Energy Basket*"

Scheuer (1974) showed that the extended powerful extragalactic radio sources require a "waste energy basket" to account for energy that is delivered by the jet to the hot spots but is not radiated away by the hot spots. We define ϵ as the fraction of jet power radiated away by the hot spot, i.e., $\epsilon \equiv L_h/Q_j$ (Hargrave & McEllin 1975). The parameter ϵ

TABLE 8

PHYSICAL PROPERTIES OF THE JETS IN 2352+495

Parameter	Symbol Used in Text	Northern Jet	Southern Jet	Ratio (north/south)
Bulk velocity ($h^{-4/7}$)	v_j	$\gtrsim 0.28c$	$\gtrsim 0.33c$	...
Energy of advance ($h^{-17/7}$ ergs)[a]	W_a	1.2×10^{53}	2.0×10^{53}	0.6 ± 0.4[c]
Energy of advance ($h^{-17/7}$ ergs)[b]	W_a	1.2×10^{54}	8.3×10^{53}	1.4×0.6[c]
Power of advance ($h^{-10/7}$ ergs s^{-1})[a]	Q_a	$1.3 \times 10^{42}\ (\tau_j/3000\ \text{yr})^{-1}$	$2.1 \times 10^{42} (\tau_j/3000\ \text{yr})^{-1}$	0.6
Power supplied to lobe ($h^{-10/7}$ ergs s^{-1})	Q_l	$6 \times 10^{42} (\tau_j/3000\ \text{yr})^{-1}$	$1.1 \times 10^{43}\ (\tau_j/3000\ \text{yr})^{-1}$	0.5
Jet power ($h^{-10/7}$ ergs s^{-1})	Q_j	3.4×10^{43}	3.0×10^{43}	1.1
Jet thrust ($h^{-10/7}$ dyn)	F	9×10^{32}	8×10^{32}	1.1 ± 0.3[c]
Radiative efficiency in hot spot ($h^{-4/7}$)	ϵ	0.07–0.23	0.04–0.12	0.6–6
Time to supply lobes ($h^{-3/7}$ yr)	τ_{supply}	1500–6500	2500–7500	0.2–2.6
Synchrotron lifetimes of lobes ($h^{-3/7}$ yr)	τ_{synch}	1200	1800	0.7

[a] Assuming no precession.
[b] With precession (see text).
[c] Assuming uncorrelated errors of 10% in the radii of the hot spots and in the flux densities and 5% in distance of the hot spots from the central component.

may be thought of as a measure of the radiative efficiency in the hot spots. The derived efficiencies for the northern and southern hot spots are given in Table 8. We see that the fractions of power radiated away in the hot spots of 2352+495 are in the range 4%–23%. Thus, a repository of the "waste" energy—identified here with the lobes (see eq. [3])—is needed for the CSOs just as it is for LSOs. Any evidence of a larger waste energy basket, such as a halo, would indicate that the activity has been ongoing in this object over a period much longer than the time required to provide the lobe energy, which is about 3000 yr (see § 7.2). We might expect the magnetic field in the halo to be lower than in the lobes and, thus, that the synchrotron loss timescale would be longer. As we saw in § 3.1.2, there is no such halo. If this object had been active for more than a few thousand years, as might be the case if it were confined in an unusually dense interstellar medium, we would expect it to have a more spherical morphology, as found in the simulations of De Young (1993). However, this is not seen in any CSO, and we conclude that these objects are unlikely to be much older than the time required to supply the energy to the lobes. We note, however, that the absence of a halo is a necessary–but not a sufficient—condition to prove that these objects are young.

5.3. *Comparison with Large FR II Objects*

Rawlings & Saunders (1991) have shown that large FR II objects have jet powers which range from 10^{44}–10^{47} ergs s^{-1} (see Fig. 4). The power deduced for the jets is comparable to the maximum-detected power output over all bands of radio-loud active galaxies. The jet power therefore provides a good estimate of the power output of the central engine. The radio power of the most luminous large FR II objects is typically a few percent of the jet power. In some objects, like Cygnus A, this ratio is as high as 20%, and this is probably due to the unusually high density of the external medium around this object.

In 2352+495, the ratio of the total power radiated at radio wavelengths to the combined power of the two jets is $\geq 0.75\ h^{-4/7}$. If we exclude the bright jet component and consider only the radio emission from the hot spots, lobes, and cocoon, the ratio is $\geq 0.33\ h^{-4/7}$—which is a remarkably high value. The higher radiative efficiency in CSOs could be caused by a stronger interaction with the surrounding medium than occurs in most large FR II objects (see, e.g., Gopal-Krishna & Wiita 1991). This appears likely since the interstellar medium surrounding the CSOs is much denser than the extragalactic medium through which the large FR II jets are propagating.

5.4. *"S-shaped" Morphology*

The radio structure of 2352+495 has S-symmetry—a property which this object has in common with 0108+388 and 0710+439 and with the CJ2 CSO 1946+708 (Taylor, Vermeulen, & Pearson 1995). This symmetry can be seen most clearly in the full resolution 1.66 GHz image (Fig. 1*e*). It could be due to precession of the central engine. Precession has previously been invoked to explain symmetries observed in large-scale radio structure (e.g., Miley 1980; Ekers 1982; Gower et al. 1982; Hunstead et al. 1984). Since S-symmetry is seen in four CSOs, while C-symmetry is seen in none, it is unlikely that the symmetry is due to either the "fire-hose" instability or the helical Kelvin-Helmholtz instability, unless these are driven by precession, and we do not consider these possibilities further.

Precession of the jet axis could be due to a binary black hole in the nucleus. For example, a binary consisting of a 10^6 and a $5 \times 10^5\ M_\odot$ black hole with separation of a few

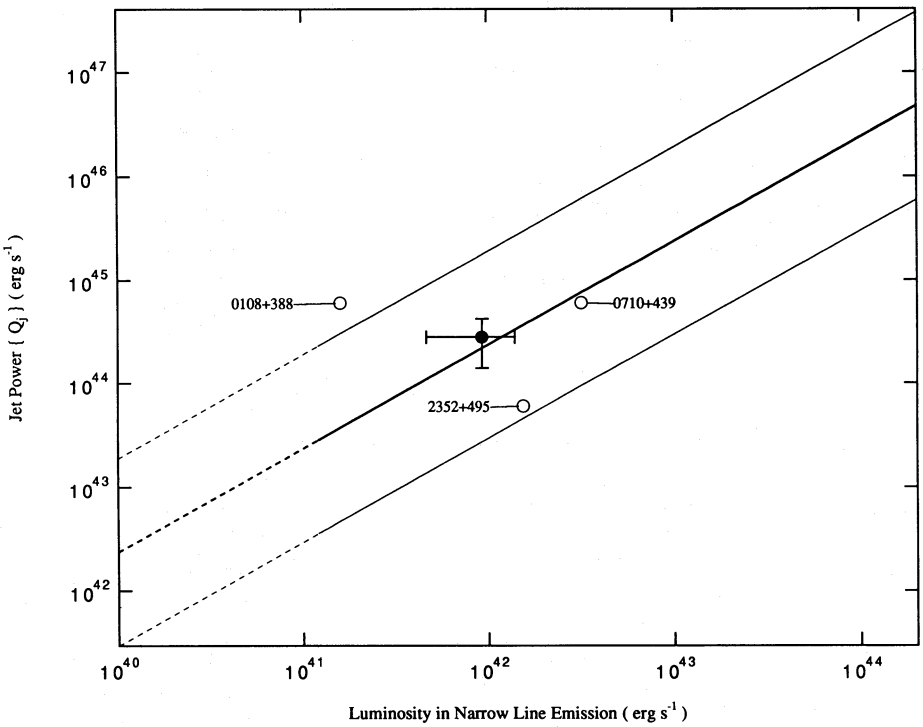

FIG. 4.—Jet power and narrow line luminosity. The jet power and the narrow line luminosity of 0108+388, 0710+439, and 2352+495 are shown. The filled circle is the geometric mean of the three observed points. The range in jet power and narrow line luminosity determined by Rawlings & Saunders (1991) is shown for a sample of FR I objects (*dashed line*) and FR II objects (*solid line*).

tenths of a parsec would have a precession period of ~ 7000 yr, whereas for two black holes of masses 10^6 and $10^8\ M_\odot$ the precession period is $\sim 2 \times 10^5$ yr (Begelman, Blandford, & Rees 1980). Both systems could survive for a Hubble time.

If the jets in 2352+495 are indeed precessing, the estimates in § 5.1 of the work done by the hot spots in advancing through the interstellar medium require modification. The work done by the advancing hot spot must now be written $W_a = pA_p d$, where A_p is the total area of the advancing working surface averaged over the radio source lifetime, and replaces A, the working surface area of the hot spot used previously. We set $\zeta = A_p/A$. Then the work done by the advancing hot spot is simply ζ times the work done in the case of no precession, calculated in § 5.1. The maximum value of A_p is obtained if the precession period is short compared with the age of the radio source. In this case we find $\zeta_n = 10$ and $\zeta_s = 4$ for the northern and southern jets. Hence we derive the values given in Table 8. Again, we see that the ratio of the work done by the two jets against the interstellar medium is close to unity.

Another feature of 2352+495 which merits comment is that the northern hot spot is not at the end of the lobe. Projection effects plus variations in the jet axis and in the density of the interstellar medium could explain this. For example, the hot spot may act like a "dentist's drill" (Scheuer 1982) and drill out a new channel, starting from further back if the direction of the jet varies.

6. THE DENSITY OF THE EXTERNAL MEDIUM

The working surfaces in CSOs are much closer to the central engine than those of any other powerful extragalactic radio sources. They therefore provide a unique probe of the interstellar medium in the distance range ~ 1 pc to ~ 1 kpc from the central engines in active galaxies. In this section we use the ram pressure confinement of CSOs to study the interstellar medium of this interesting region.

Our treatment here is based on the assumption of ram pressure confinement in a uniform medium (eq. [6]). This assumption merits some discussion. A light (electron-positron) jet which encounters an increase in the density of the external medium might be expected to decelerate, at least initially. It has been suggested that in compact objects the advance of the jets is slowed significantly by interactions with dense clouds (O'Dea, Baum, & Stanghellini 1991; Carvalho 1994). In the PR CSOs we observe two lobes at comparable distances (~ 50 pc) from the centers of activity (see Fig. 1). Thus, if dense clouds determine the speed of advance, then in order to account for the arm length ratios observed in this sample, the mean free path between the clouds must be $\ll 100$ pc. If the clouds are larger than the hot spots, i.e., $\gtrsim 10$ pc, the fraction of the volume filled by clouds is about the ratio of the cloud diameter to the mean free path between clouds, so that for our objects the fraction of the volume filled by clouds must be $\gg 0.1$. Thus, the assumption of a uniform medium is justified for clouds larger than the hot spots. It has also been shown in simulations of multiple encounters of light jets with large clouds (De Young 1991, 1993; 1995, private communication) that the clouds do not slow the jet for significant periods. If the clouds are smaller than the hot spots, cloud evaporation can occur, and this can add significant mass to the jet and hence slow it down. In this case momentum conservation leads to equation (6), and it can be shown that for a given advance speed of the jet the mean external density is a minimum in the case of a uniform medium. Thus, the conservative approach is to assume a uniform medium. For these reasons we consider only a uniform medium in the following discussion.

6.1. *Ram Pressure Confinement in a Uniform Medium*

We consider two models for 2352+495. In our first model we assume an advance speed for the hot spots of $0.02c$, and in our second model we assume an advance speed of $4 \times 10^{-3}c$. We refer to these as the fast and slow models. The average pressure in the two hot spots and the ram pressure relation of equation (6) shows that the densities in the external medium on these two models are 10 and 300 cm^{-3}. The values of the relevant parameters for the two models are given in Table 9. These have been derived as described below.

It is useful for the following discussion to parameterize the equations in terms of a value for v_a of $0.02c$. The hot-spot pressure we use is based on the assumption of equipartition between particle and magnetic field energy densities, which are very close to the minimum energies; hence, it is a lower limit, and, consequently, the densities and masses derived below are also lower limits. From equation (6) we calculate the density of the interstellar medium required to provide the ram pressure braking. The value that we determine from the mean pressure of the northern and southern hot spots of 2352+495 is

$$\rho_{\mathrm{ext}} = 2 \times 10^{-23} \left(\frac{v_a}{0.02c}\right)^{-2} h^{4/7}\ \mathrm{g\ cm^{-3}}\ ,$$

i.e., we need a proton density of

$$n_p = 10 \left(\frac{v_a}{0.02c}\right)^{-2} h^{4/7}\ \mathrm{cm^{-3}}\ .$$

We show in Paper III that the speed of advance of the hot spots in these objects is independent of the external density. Given a constant expansion speed, if the luminosities of CSOs were independent of their overall size, we would expect the number of CSOs in a complete flux-density–limited sample to increase by a factor of 10 for each decade in overall size. We saw in § 2 and in Table 2 that this is certainly not the case. *Therefore, the luminosity of CSOs must decrease significantly with increasing size.* We will return to this discussion of the evolution of CSOs in Paper III. For the present we will adopt a simple model in which the luminosity of CSOs is assumed constant for hot spot separations up to R_{const} and then drops precipitously. On this model, CSOs will be observed on average when their separation from the core is $0.5R_{\mathrm{const}}$. In an orientation-unbiased sample, the actual size is $4/\pi$ times the average projected size. Thus $R_{\mathrm{const}} = 8/\pi$ times the average observed core–hot spot separation. From the five CSOs in the PR sample, we find $R_{\mathrm{const}} \approx 200\ h^{-1}$ pc. A region of the above density $200\ h^{-1}$ pc in radius has mass, M_c, given by

$$M_c \sim 10^7 \left(\frac{v_a}{0.02c}\right)^{-2} h^{-17/7}\ M_\odot\ . \qquad (7)$$

6.2. *Observational Limits on the External Density*

We have made a number of observations for the purpose of estimating, or placing limits on, the external gas density. We consider a confining cloud composed of pure hydrogen

TABLE 9

JET AND CONFINING MEDIUM ON THE TWO MODELS FOR 2352+495

Parameter	Symbol Used in Text	Slow Jet	Fast Jet
Age (yr)	τ_j	5×10^4	9000
Velocity of advance	v_a	$4 \times 10^{-3}c$	$0.02c$
Density of ISM (cm^{-3})	n_p	300	10
Mass of Confining Cloud($M_\odot$)	M_c	3×10^8	10^7
H I Column Density (cm^{-2})[a]	N_{HI}	2×10^{23}	8×10^{21}
Optical Depth in H I[b]	$\tau(v)$	1	0.05

[a] Assuming a neutral cloud of radius 200 pc.
[b] Assuming $\delta v = 700$ km s^{-1} and spin temperature $T_s = 100$ K.

in thermal equilibrium with the radiation field at temperature T. We use the Saha equation to determine the loci in the (T, n_p)-plane for two levels of ionization—$N(\text{H II})/n_p = 0.01$ and $N(\text{H II})/n_p = 0.99$, where $n_p = N(\text{H I}) + N(\text{H II})$. The loci corresponding to the 1% and 99% ionization conditions are shown in Figure 5. We first consider the possibility that the temperature of the confining cloud is greater than $\sim$4000 K, in which case the medium is almost fully ionized, and we then consider the possibility that the confining medium is cooler, and predominantly neutral, gas.

6.2.1. *The Ionized Gas Density*

We saw, in § 3.2.1, that $\tau_{0.151}^{\text{free-free}} < 1$. This limit in optical depth at 151 MHz gives a lower limit to the temperature of the confining cloud if the cloud is ionized. In Figure 5 we have plotted this limit for an assumed path length of 100 pc through the ionized medium. We see that on the slow model the temperature must exceed 4×10^5 K if the medium is ionized.

The X-ray observations can also be used to place limits on the temperature and density of the confining medium. A discussion of the constraints on X-ray luminosity provided by the X-ray observations is given by O'Dea et al. (1995). If the temperature of the confining cloud is greater than 4000 K, then it will be ionized and the upper limit in X-ray luminosity rules out the region of the (T, n_p)-plane to the right of the curve marked "X-ray Limit" in Figure 5. If the temperature and pressure of the cloud lay in the portion to the right of this curve, the X-ray luminosity would exceed

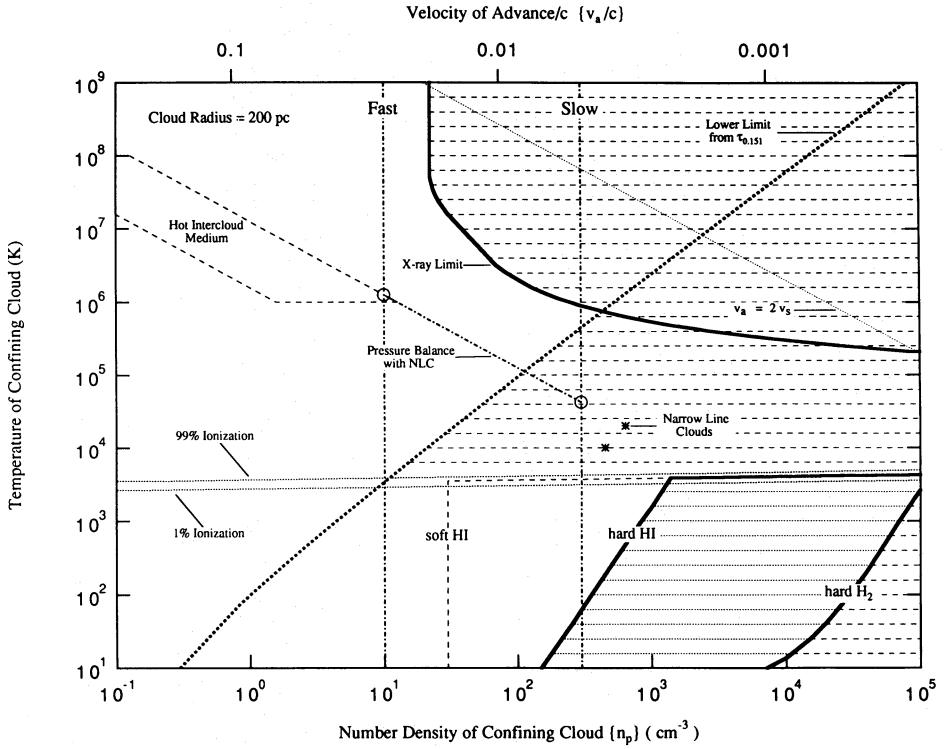

FIG. 5.—Temperature–number density plot for the confining cloud in 2352+495. The corresponding velocity of advance derived from the mean hot spot pressure is shown on the top axis. We assume a cloud radius of 200 pc (see text). The upper limit to the optical depth at 151 MHz provides a lower limit to the temperature for an ionized cloud. The upper limit to the X-ray luminosity excludes the portion of the T-n_p plane to the right of the X-ray curve. Also shown are the densities on the fast and slow models, and the hard and soft limits provided by the H I absorption observations and the hard limit provided by CO absorption observations. The region occupied by the narrow line clouds is shown by the two starred points, which correspond to temperatures of 10,000 K and 20,000 K. The region occupied by the "hot intercloud medium" is also indicated. The locus for an external medium in pressure equilibrium with the narrow line clouds is shown by the line marked "Pressure Balance with NLC." The locus for a medium in which the advance speed is twice the external sound speed is also indicated. The region with horizontal dashes is absolutely excluded, and the region with horizontal dotted lines is excluded for H I but not for H_2 (see text).

the maximum permitted luminosity of $3.4 \times 10^{42}\ h^{-2}$ ergs s^{-1} determined by O'Dea et al. (1995) after taking account of Galactic absorption. The portion of the (T, n_p)-plane that is excluded by the upper limit in optical depth at 151 MHz and by the upper limit in X-ray luminosity is indicated by dashed horizontal hatching in Figure 5. We see that on the slow model there is only a small range of temperature (from 4×10^5 to 10^6 K) which does not conflict with either the X-ray limit or the optical depth limit at 0.151 GHz. However, a two-phase medium with a hot phase at this temperature and density cannot be maintained in equilibrium (e.g., Netzer 1990). So this solution is unphysical. Thus, on the slow model the medium must be predominantly neutral, and the contribution of any ionized gas to hot spot confinement is insignificant. Note that if there is significant H I in the confining cloud, the temperature must be less than 4000 K and the cloud would absorb X-ray emission. We discuss the possibility of a neutral confining cloud in the following section.

The fast model is consistent with a photoionized "Hot Intercloud Medium" in pressure equilibrium with the narrow line clouds, as shown in Figure 5, and such a two-phase medium can be maintained in equilibrium (Netzer 1990). The line marked "Pressure Balance with NLC" in Figure 5 shows the locus of points in pressure balance with the narrow line clouds at 2×10^4 K. The densities corresponding to the two points marked "Narrow Line Clouds" have been calculated from the ratio of the [S II] λ6716 and λ6731 lines for the temperatures 10^4 and 2×10^4 K (see § 4.2).

It is possible that useful limits on the density in ionized gas might be provided by polarization observations. A characteristic feature of CSOs, as pointed out in § 2, is their low radio polarization. Rudnick & Jones (1983) place 2 σ upper limits on the integrated polarization in 2352+495 of less than 0.12% at 5 GHz and less than 1.1% at 15 GHz. In addition, observations at 8.4 GHz have detected polarization at the 0.2% level (I. W. A. Browne 1995, private communication). Using VLBI techniques, Cawthorne et al. (1993) found no polarized flux in excess of 3 mJy $beam^{-1}$, which corresponds to less than 3% for the bright jet feature and less than 15% for the northern hot spot.

The very low polarization observed in 2352+495 may be the result of (1) a highly "tangled" magnetic field within the source, (2) depolarization by a dense thermal gas intermixed with the radio-emitting plasma, or (3) depolarization by an external Faraday screen. The first possibility is unlikely, since any shear or compression will strongly polarize the radio source (Laing 1980). Given the morphology of the source and its large equipartition pressures, shear and compression are likely to occur. Internal Faraday depolarization requires an intermixed thermal material with density greater than 0.01 cm^{-3}. Although internal Faraday rotation has not been detected in larger jets, CSO jets are propagating through a much denser environment, and they may interact with their environs more strongly—so this seems a plausible explanation for the low polarization of CSOs.

Depolarization by an external Faraday screen of the signal within the VLBI beam of Cawthorne et al. ($\sim$2 mas) requires rotation measure (RM) gradients greater than 10^5 rad m^{-2} $arcsec^{-1}$. This is an order of magnitude greater than the largest RM gradient found in kiloparsec-scale radio sources (e.g., 3C 295—Perley & Taylor 1991; Hydra A—Taylor & Perley 1993). For a uniform magnetic field, B, and density, n_e, in a Faraday screen of depth L, we have

$$L n_e B > 250 \text{ kpc cm}^{-3} \mu\text{G} .$$

For a path length of 200 pc (see § 6.1) and field strength of 100 μG, the electron density required is 40 cm^{-3}. This is significantly larger than the density deduced from the narrow line reddening in the following section. For both internal and external Faraday depolarization, sensitive VLBI observations at high frequencies should recover the intrinsic polarization of the source. Such observations are being carried out for 2352+495 and other CSOs.

6.2.2. *Neutral Gas Density*

An estimate may be made of the neutral gas density in the narrow emission-line region from the reddening of the Balmer lines. The reddening of the narrow emission-line regions is significantly greater than the reddening of the underlying continuum of galactic stars (see § 4.2), which indicates that there is significantly more dust in the narrow line region than in the surrounding galaxy. The increased reddening toward the narrow lines implies a gas column density in the narrow line region of 2×10^{21} cm^{-2} for a medium with the same extinction properties as our Galaxy and a λ^{-1} extinction law (Netzer 1990). For a confining medium 200 pc in extent (see § 6.1), this implies a density of $\sim$3 cm^{-3} for the interstellar medium within a few hundred parsecs of the central engine in 2352+495.

If the gas-to-dust ratio, or the extinction law, is significantly different from that in our Galaxy, it is possible that the density in neutral gas is significantly greater than $\sim$3 cm^{-3}. In this case, the confining cloud might be maintained in equilibrium by the same mechanism which obtains in extremely luminous infrared galaxies such as Arp 220 and Mrk 231 (Soifer et al. 1984; Scoville et al. 1989; Sanders, Scoville, & Soifer 1991; Scoville 1994). In these objects there is evidence of massive neutral clouds which are thought to be in equilibrium, but in which the mechanism by which this equilibrium is maintained is not understood.

If CSOs are confined by a neutral gas cloud consisting primarily of atomic hydrogen, the H I should be observable in absorption against the compact radio continuum source. We have carried out H I observations of 2352+495 with the VLBA. Spectra integrated over the northern lobe, over the bright jet region, and over the southern lobe are shown in Figure 6*b*. There is no evidence of absorption, and it is clear that the optical depth along the lines of sight to all three components is less than 5%.

If the narrow line region is cospatial with the 200 pc cloud and has the same kinematics, we may use the optical line widths to estimate the dispersion in velocity of the H I. As can be seen in Table 7, there is a considerable spread in the narrow line widths. We assume a width of 700 km s^{-1}—equal to the FWHM of the [O III] lines. To estimate the radiative pumping, we use the mean brightness temperature of the radiation field at the rest-frame frequency of 1420 MHz, assuming that this is dominated by the hot spots at a distance of 50 pc. We assume a completely neutral medium since this gives the most conservative upper limit on n_p. With these assumptions, we have used our upper limit on the optical depth and the expression given by Field (1958) for the spin temperature (which takes account of atomic collisions and radiative pumping) to solve for the spin temperature and the limit on n_p as a function of the gas tem-

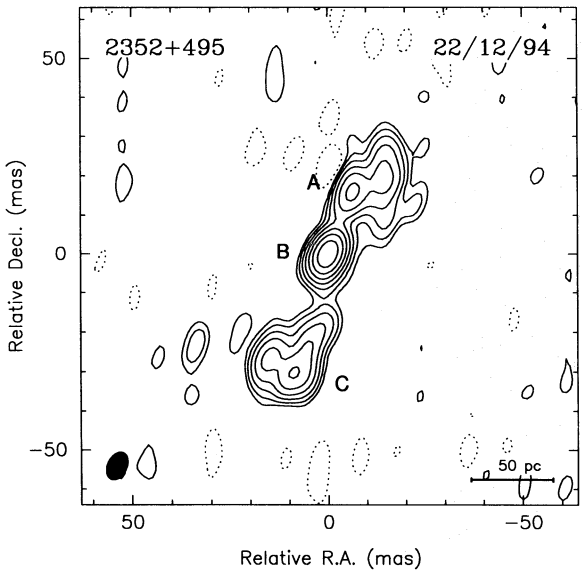

FIG. 6a

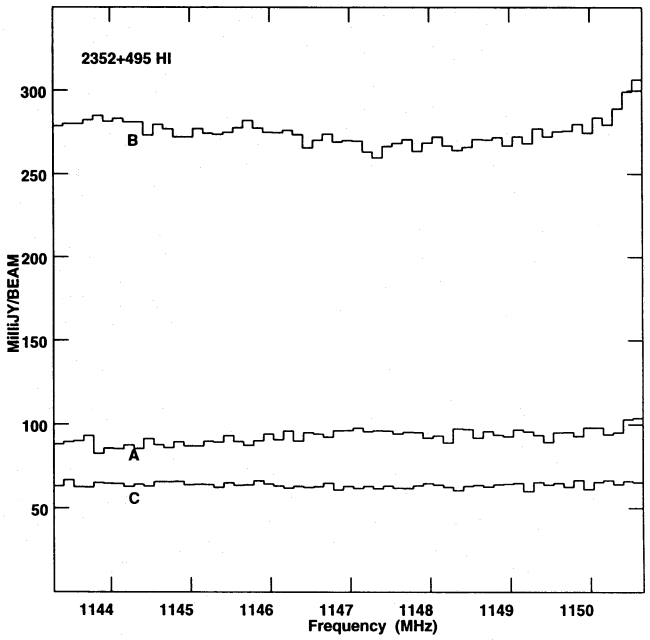

FIG. 6b

FIG. 6.—(*a*) Continuum image of 2352+495 at 1147 MHz. Contours are at intervals of 2 starting at 2 mJy beam^{-1}. The beam size, plotted in the lower left-hand corner, is 7.46 × 4.83 mas^2 in p.a. of −25°. (*b*) Spectra at the frequency of the redshifted H I line for the three components indicated in (*a*). The systemic redshift corresponds to a frequency for H I of 1147.9 MHz. The velocity resolution is 33 km s^{-1}, and the total velocity range covered in the spectra is 1900 km s^{-1}.

perature. The results are shown by the curve labeled "hard" in Figure 5. Note that at a temperature of the gas of 10^3 K the upper limit on the density of H I in the narrow line region is ~800 cm^{-3}. The above values are rather extreme compared with the situations in those cases where H I is observed in absorption near an active galaxy nucleus (see below). We have therefore also calculated the limiting density in H I for the case of a spin temperature of 1000 K and a line width of 200 km s^{-1}, corresponding to the narrowest optical emission line widths. With these values we derive a soft upper limit on the H I column density of 2×10^{22} cm^{-2}, i.e., a soft upper limit of 30 cm^{-3} for the density of H I in the narrow line region. The corresponding limit is shown by the line marked "soft" in Figure 5. We see that the hard limit does not exclude either of our models, while the soft limit strongly excludes the slow model but is consistent with the fast model.

We have searched the literature for reports of evidence of H I absorption in other elliptical galaxies. The most detailed study carried out thus far is that of van Gorkom et al. (1989, 1990). These authors observed a complete sample of 29 elliptical galaxies with compact radio cores, and they detected H I absorption in four systems—0116+319, 1003+351 (3C 236), 1146+596 (NGC 3894), and 1353+056 (NGC 5367). Their results are summarized in Table 10. By comparing these results with the model predictions of Table 9, we see that the observed H I clouds in elliptical galaxies at low redshifts have significantly lower column densities and optical depths than even the fast model limit, and differ from the slow model limit by over 2 orders of magnitude. In all four cases, the observed H I clouds are redshifted relative to the optical galaxy, so that they are falling in toward the center of the galaxy and are, therefore, very likely the source of the fuel for the nuclear activity. In elliptical radio galaxies with extended continuum emission, the absorption system is seen only against the compact central component (van der Hulst, Golisch, & Haschick 1983; Shostak et al. 1983) which shows that the absorbing clouds are very close to the nucleus. The estimated infall rates are a few hundredths of a solar mass per

TABLE 10

PROPERTIES OF CLOUDS OBSERVED IN ELLIPTICAL GALAXIES[a]

Object	N_{HI}[b] (cm^{-2})	τ	Line Width (km s^{-1})	Velocity Offset from Galaxy (km s^{-1})
0116+319	10^{21}	0.04	153	−212
1003+351 (3C 236)	8×10^{20}	0.03	133	−162
1146+596 (NGC 3894)	2×10^{21}	0.04	109	−17
1353+055 (NGC 5363)[c]	5×10^{20}	0.01	45	−22
	5×10^{20}	0.01	49	−96

[a] See van Gorkom et al. 1989, 1990.
[b] Assuming a spin temperature of $T_s = 100$ K.
[c] This object has two absorption lines.

year, which is comparable to the accretion rate required to fuel 2352+495 (see § 9). Two of the four objects detected in H I absorption by van Gorkom et al. (1989, 1990), 0116+319 and 1148+596, are CSO candidates (Taylor et al. 1994; Dallacasa et al. 1995) and a third, 1003+351, has a CSO-like central component, although it does have FR II structure on much larger scales (Barthel et al. 1985).

It is possible that the confining medium in CSOs is primarily molecular and might not, therefore, be readily observable in absorption by H I or by free-free absorption. We have made observations of 2352+495 in CO on the Owens Valley Radio Observatory (OVRO) millimeter array. Our observations (Fig. 7) show no evidence of absorption and provide an upper limit on the optical depth of $\tau < 0.1$ (3 σ). In situations which obtain in normal galaxies, this limit on CO absorption optical depth would provide a stringent limit on the density of H_2: For an excitation temperature of 20 K, a line width of 700 km s^{-1}, and an H_2/CO ratio of 10^4, this implies a column density of less than 2×10^{21} cm^{-2}, i.e., an upper limit on the H_2 density of 3 cm^{-3}. However, as has been pointed out by Maloney, Begelman, & Rees (1994) and by Barvainis & Antonucci (1994), it is possible for radiative pumping of the molecular levels by the millimeter and submillimeter nonthermal radiation in the nuclear regions of an active galaxy to increase the excitation temperature and hence significantly reduce the absorption optical depth in CO. This is the same process as that discussed by Field (1958) for the case of H I. We have carried out the calculation for the hot spots in 2352+495. The brightness temperatures of the two hot spots at an emitted frequency of 115 GHz, assuming that the high-frequency spectral indices continue as $\alpha = -0.5$ up to this frequency, are $\sim 10^6$ K, corresponding to an effective radiation temperature of ~ 800 K at a distance of 50 pc.

The situation in 2352+495 is somewhat different to that in Cygnus A because the density of the absorbing cloud is much lower in 2352+495, and, consequently, spontaneous de-excitation is not negligible compared to collisional excitation and de-excitation. We have used the collisional rate constants determined by Schinke et al. (1985), and taken the spontaneous emission into account in calculating the upper limit to the molecular gas density as a function of gas temperature and assuming a line width of 700 km s^{-1}. The upper limit is shown by the curve labeled "hard H_2" in Figure 5.

In summary, we can place fairly stringent limits on the density of the ionized gas ($n_p \lesssim 450$ cm^{-3}) in the confining cloud based on the upper limit of the free-free optical depth at 151 MHz and the upper limit of the X-ray luminosity, and we can place fairly stringent limits on the density of the atomic gas ($n_{\rm H\,I} \lesssim 1000$ cm^{-3}) in the confining cloud based on the lack of H I absorption, but we cannot place stringent limits on the density of the molecular gas in the confining cloud since, for molecular densities below 10^5 cm^{-3}, any such material would be strongly excited by radiation from the hot spots.

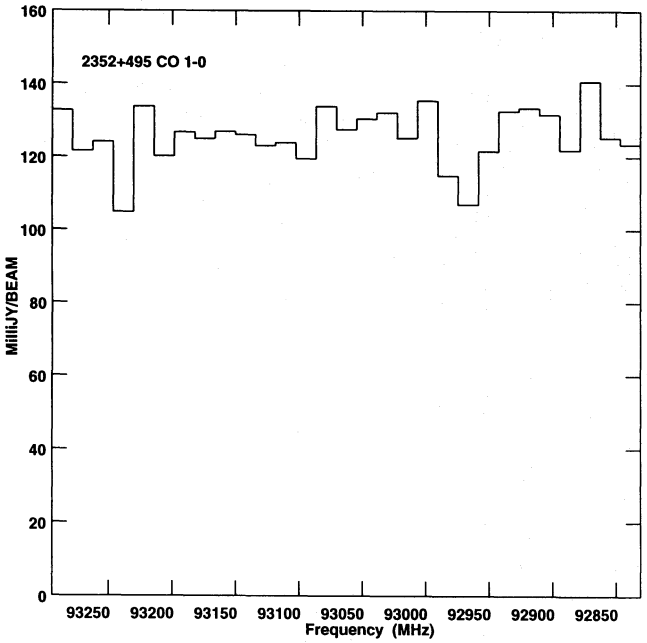

FIG. 7.—Spectrum at the frequency of the redshifted CO $J = 1$–0 transition for 2352+495 obtained with the OVRO millimeter array from a 12-hr observation in 1995 March. The systemic redshift corresponds to a frequency for CO 1–0 of 93090 MHz. The velocity resolution is 52 km s^{-1}, and the total velocity range covered in the spectrum is 1500 km s^{-1}.

6.3. *Expansion Speeds and Simulations*

Lind et al. (1989) have carried out simulations of relativistic jets which show that the terminal speed of advance is $v_a \sim 2v_s$, where v_s is the sound speed in the external medium. This suggests that v_a is independent of $\rho_{\rm ext}$ but depends explicitly on $T_{\rm ext}$, the temperature of the external medium. This would be consistent with the fast model if the temperature in the external medium of CSOs were the same as the temperature in the external medium of LSOs. We have calculated the advance speed of the hot spots of 2352+495 on this theory—the relevant relationship is shown by the line labeled "$v_a = 2v_s$" in Figure 5. The implied temperatures at densities below 10^5 cm^{-3} exceed 10^5 K, so the medium would be ionized, and the limits provided by the X-ray and free-free calculations of § 6.2.1 may be applied. We see that the temperature must exceed 10^9 K—much larger than the temperatures thought to obtain in the narrow line regions or even in the hottest known clusters of galaxies. The ram pressure results for CSOs are therefore not consistent with the results of the simulations of Lind et al. (1989), since the implied temperatures are much too high, so that these simulations appear not to provide a good description of the jets in CSOs.

6.4. *External Densities—Conclusion*

The constraint on the ionized material provided by the limit on free-free absorption and X-ray luminosity shows that $n_p \lesssim 450$ cm^{-3}, while the absorption measurements provide an upper limit on $n_{\rm H\,I}$ of 1000 cm^{-3}. Due to the radiative excitation of CO by the hot spots, the limit on the density of molecular material is much weaker ($n_{\rm H\,II} \lesssim 10^5$ cm^{-3}). All of these results provide only upper limits on the density. The only actual value that we have measured, as opposed to limits, is the additional reddening in the narrow line clouds, which yields a gas density of 3 cm^{-3} in 2352+495. Evidence which is independent of the ionization state of the external medium may be gained from the ram pressure arguments of § 6.1. In Paper III we show that, provided we have identified the centers of activity correctly, the expansion velocities of CSOs are independent of the external densities and, hence, that the hot spot pressure is proportional to the external density. The hot spot pressures

in CSOs are a factor $\sim 10^4$ greater than the hot spot pressures in LSOs. The typical densities in the external medium of the LSOs we have studied are $\sim 10^{-3}$ (see Paper III). This provides independent evidence for external densities in CSOs of $\sim 10\ \mathrm{cm}^{-3}$.

Thus the likeliest scenario is that the external medium is photoionized and is simply the hot intercloud medium at a temperature of $\sim 10^6$–10^7 K and a density of $\sim 10\ \mathrm{cm}^{-3}$. We will assume from now on that the fast model applies in CSOs and, hence, that $v_a \sim 0.02c$ in these objects and is very similar to the expansion speeds in LSOs.

7. AGES AND TIMESCALES

The determination of the age of CSOs is essential for understanding these objects. We therefore now discuss the age of CSOs and the timescales of various processes which determine the age. We will show that the ages are certainly $\ll 10^6$ yr and that the observational evidence strongly favors ages of $\sim 3 \times 10^3$–10^4 yr, although ages as high as 10^5 yr cannot be ruled out definitively. In Paper III we present an argument based on the physics of the two oppositely directed jets in CSOs which considerably strengthens the case for ages of $\sim 10^4$ yr.

7.1. *The Age of CSOs Derived from the Advance Speed*

We have carried out an analysis identical to that leading to equation (7) on the two other PR CSOs which have clearly identified hot spots in both jets (0108+388 and 0710+439), and we have derived equivalent relationships for them. The model leading to equation (7) is a conservative one in the sense that it assumes equipartition in a light (electron-positron) jet. If equipartition does not apply, or if these are heavy (electron-proton) jets, the densities and masses implied are significantly greater than the values we have derived. The most important assumptions in our argument are that the hot spots are confined by ram pressure and that this sets the advance speed. Our conclusions regarding ages all depend on these assumptions. We defer a detailed discussion of these points to Paper III. Based on these assumptions, the resulting masses rule out large ages ($\sim 10^6$ yr) for CSOs: For an age of 10^6 yr, when the hot spots are 50 pc from the central engine, the hot spot pressures give masses within 200 pc radius of $2 \times 10^{12}\ M_\odot$ for 0108+388, $8 \times 10^{11}\ M_\odot$ for 0710+439, and $2 \times 10^{11}\ M_\odot$ for 2352+495. These masses are certainly out of the question. Thus, provided these objects are confined by ram pressure, we can be certain that the PR CSOs are much younger than typical FR II objects.

Even for an age of 10^5 yr at 50 pc, the masses within a 200 pc radius are $2 \times 10^{10}\ M_\odot$ for 0108+388, $8 \times 10^9\ M_\odot$ for 0710+439, and $2 \times 10^9\ M_\odot$ for 2352+495. The mass inferred for 0108+388 is greater than the central mass concentrations within 200 pc radius of even the most extreme hyperluminous starburst galaxies. Thus these masses are highly implausible given that we see no evidence of hyperluminous starburst activity in any of these objects.

Thus the required central masses and lack of any sign of hyperluminous starburst activity in the PR CSOs point to ages significantly less than 10^5 yr for these systems, provided that they are ram pressure confined and the advance speed is set by the hot spot pressure. The overall projected size of the radio source in 2352+495, as measured on the 610 MHz map, is $\sim 170\ h^{-1}$ pc. A firm lower limit to the age of the radio source can be obtained by making the assumption $v_a = c$, which shows that $\tau_{\min} = 275\ h^{-1}$ yr. The timescale for the source to reach its present size is

$$\tau_a \sim 1.4 \times 10^4\ h^{-1} \left(\frac{v_a}{0.02c}\right)^{-1} \text{ yr} .$$

Conway et al. (1992, 1994) have shown that the advance speeds of the outer components of 0108+388, 0710+439, and 2352+495 are subluminal, with the most stringent limit ($v_a \leq 0.18\ h^{-1}c$) on 0108+388. If the age of 2352+495 is $\sim 10^4$ yr, as inferred in § 6, the hot spot advance speed is $\sim 0.02c$, or ~ 0.002 mas yr^{-1}. Such a motion should be measurable in less than 10 yr with the VLBA. Lower redshift CSOs may give results sooner.

7.2. *Timescale for Supply of Energy to Lobes*

We see from equation (3) that the bulk kinetic power supplied by the jet to the lobes and to advance the jet through the external medium is given by

$$Q_a + Q_l + Q_c/2 = (1 - \epsilon)Q_j = L_h \frac{(1 - \epsilon)}{\epsilon} .$$

We assume that the time to supply the energy to the lobes and the cocoon is the same and call this τ_{supply}. If there is negligible leakage of particles from the cocoon, $\tau_{\text{supply}} = \tau_j$, so that, for lobe energy U_l and cocoon energy U_c, we have

$$\tau_{\text{supply}} = \left(\frac{W_a + U_l + U_c/2}{L_h}\right) \frac{\epsilon}{(1 - \epsilon)} ,$$

which, for the ranges of ϵ determined above, yields ages in the range 1500–6500 yr for the northern lobe and 2500–7500 yr for the southern lobe (see Table 8). Thus the lobe supply timescales agree reasonably well with the expansion timescale we deduced in the previous section. Note that we have assumed a steady state for the jet. In reality, the source luminosity and radiative efficiency probably change with time. A more detailed model would be needed to take account of this. However, we believe that it is significant that the supply times are consistent, within the uncertainties, with the expansion times.

7.3. *Synchrotron Lifetimes*

The only components of 2352+495 in which we have any spectral evidence of synchrotron aging are the lobes and the bright jet component (see Fig. 2 and Table 6). There is a break in the lobe spectra near 5 GHz and in the bright jet feature near 15 GHz. The corresponding synchrotron loss timescales of the northern and southern lobes are 1200 and 1800 yr, respectively. These are somewhat lower than the lobe energy supply times determined above, which is to be expected since the synchrotron-loss timescale must be a lower limit to the age of the source.

7.4. *Summary of Age and Timescale Determinations*

A self-consistent picture has emerged of the age of 2352+495. The various age and timescale estimates that we have made are shown in Table 11. There are three independent age arguments: one based on the upper limits on the mass concentrated in the central 200 pc radius, one based on the external density and implied expansion speed, and one based on energy supply times. We have discussed the limits based on mass estimates thoroughly in § 7.1, so we do not discuss them further here. We saw in § 6 that the various estimates of the external density in 2352+495 are

all consistent with $\sim 10\ \mathrm{cm}^{-3}$, and thus an advance speed of $\sim 0.02c$ and an age of $\sim 10^4$ yr. The observed limit on H I absorption rules out densities $\gtrsim 1000\ \mathrm{cm}^{-3}$ in H I. The observed limits on free-free absorption at 151 MHz and X-ray luminosity also rule out densities significantly greater than $450\ \mathrm{cm}^{-3}$ in H II. Thus, these limits imply ages less than 10^5 yr if the confining cloud is either ionized or atomic. We have not been able to rule out, on the basis of CO observations, the possibility that the confining medium is a dense ($n_{\mathrm{H}} \sim 10^5\ \mathrm{cm}^{-3}$) molecular cloud, since the CO is very likely radiationally excited by millimeter continuum radiation from the hot spots. The different reddening observed in the narrow lines and the galaxy continuum implies a density corresponding to an age of 7500 yr if the host galaxy of 2352+495 has the same extinction properties as our Galaxy and a λ^{-1} extinction law.

The age derivation based on energy supply times is a strong argument, provided there is not much leakage of particles from the lobes and cocoon. The absence of a halo is a necessary, but not sufficient, indication that there is not much leakage. It is therefore consistent with the interpretation that the time required to supply the energy to the lobes provides an estimate of the age of the radio source in 2352+495. Further support for this interpretation is provided by the morphology of CSOs, which is very similar to that of LSOs, and does not have the more spherical halo suggested by the simulations of De Young (1993). The agreement in the ages derived by our three independent arguments is good, and we believe that there is little doubt that CSOs are young, with typical ages 3×10^3–10^4 yr, i.e., almost certainly $\ll 10^5$ yr, and that the speed of advance of the jets through the interstellar medium is $\sim 0.02c$.

8. IMPLICATIONS OF THE LOW AGE OF CSOS

8.1. *The Space Density of CSOs and Their Parent Objects*

The five CSOs in the PR sample all lie in the redshift range 0.2–0.7. The number of confirmed CSOs is too small to investigate their cosmological evolution at this point, but it should be possible to do this once the candidate CSOs from the CJ1 and CJ2 surveys have been confirmed or rejected. For the present we assume that CSOs are uniformly distributed, and we estimate the space density of CSOs from those in the PR survey, i.e., those with $S_{5\ \mathrm{GHz}} \geq 1.3$ Jy, as

$$N_{\mathrm{cso}}^{1.3} = \sum_{\mathrm{PR}} (V_m)^{-1} ,$$

where the sum extends over the CSOs in the PR survey and V_m is the volume over the area of the PR survey enclosed by the distance at which the flux density of the CSO would equal the PR survey limit of 1.3 Jy. Hence, we find $N_{\mathrm{cso}}^{1.3} = 5 \times 10^{-9}\ h^3\ \mathrm{Mpc}^{-3}$.

The redshift range of the PR CSOs shows that these objects appeared between $2 \times 10^9\ h^{-1}$ and $5 \times 10^9\ h^{-1}$ yr ago. Thus, the period of formation of CSOs lasted between $3 \times 10^9\ h^{-1}$ and $6 \times 10^9\ h^{-1}$ yr (the age of the universe). We assume a timespan of τ_{PR} for a CSO in the high-luminosity phase. Thus $\tau_{\mathrm{PR}} \sim 10^4$ yr, and the probability of observing an object in its CSO phase is $P_{\mathrm{cso}} \sim \tau_{\mathrm{PR}}/(3 \times 10^9) \sim 3 \times 10^{-6}$.

It is possible that the activity that we see in CSOs is recurrent. This possibility has been considered for GPS objects by Baum et al. (1990), O'Dea et al. (1991), and Stanghellini et al. (1990, 1993). In the case of CSOs, such recurrences must be separated by a period of time which is sufficiently long for the previous activity to have ceased—any channel through the interstellar medium should have closed, otherwise the period of continuous activity in these objects would be much longer than 10^4 yr. If we assume that a typical CSO passes through η active phases, the space number density of parent objects for CSOs is $N_{\mathrm{P_{cso}}}^{1.3} = N_{\mathrm{cso}}^{1.3}/(\eta P_{\mathrm{cso}}) \sim 15\ \eta^{-1}\ \tau_{\mathrm{PR}}^{-1}\ h^3\ \mathrm{Mpc}^{-3}$. Thus, each event will have sufficient time ($\sim 10^5$ yr) to die away before the next one occurs only if $\eta \lesssim 3 \times 10^4$. Thus we can place an upper limit on η of 3×10^4, and hence $N_{P\mathrm{CSO}}^{1.3} > 2 \times 10^{-7}\ h^3\ \mathrm{Mpc}^{-3}$.

We saw in § 4.2 that the host galaxy of 2352+495 has luminosity $\sim 0.35\ L^*$. To calculate the space number density, N_E, of elliptical galaxies with $L > 0.35\ L^*$, we use the luminosity function of Efstathiou et al. (1988). We assume that CSO hosts are elliptical galaxies and that one third of the galaxies with $L \sim L^*$ are elliptical galaxies (Begelman, Blandford, & Rees 1984). Hence we find $N_E \sim 4 \times 10^{-3}\ h^3\ \mathrm{Mpc}^{-3}$. If a fraction ξ of elliptical galaxies brighter than $0.35\ L^*$ exhibit CSO activity, we have $\eta\xi\tau_{\mathrm{PR}} \sim 4 \times 10^3$ yr. Thus the limits $1 \leq \eta \lesssim 3 \times 10^4$ imply $10^{-4} \lesssim \xi \leq 1$. If $\eta \sim 1$, CSO activity must occur in almost all elliptical galaxies with $L > 0.35\ L^*$, i.e., if CSO activity occurs typically only once in a galaxy then a large fraction of bright elliptical galaxies must exhibit this behavior.

8.2. *The "Frustrated Jet" Model*

We have shown that CSOs are almost certainly small

TABLE 11

TIMESCALES IN 2352+495

Relevant Timescale	Method	Parameters Used in Text	Age or Timescale (yr)
τ[a]	Mass limit	d and n_p	$\ll 10^6\ h^{3/14}$
τ_j[b]	Advance	d and v_a	$< 10^5\ h^{-1}$
τ_j[c]	Advance + reddening	d and v_a	$7500\ h^{-1}$
τ_{supply}[d]	Energy supply	Q_j, L_h, and U	$(1500$–$7500)\ h^{-3/7}$
τ_{synch}	Synchrotron loss	ν_c	$(1200$–$1800)\ h^{-3/7}$
τ_{min}	Minimum	d and c	$> 250\ h^{-1}$
τ_c	Characteristic	U_{min} and L	$2500\ h^{-3/7}$

[a] Assumes ram pressure confinement of hot spots.
[b] Assumes the confining medium is predominantly H I or H II.
[c] Assumes the same extinction properties in 2352+495 as in our Galaxy and a λ^{-1} extinction law.
[d] Assumes no leakage of energetic particles from the lobes.

because they are young and not because they have been held back by ram pressure braking in an unusually dense interstellar medium. The "frustrated jet" model has been suggested as an explanation of CSOs and MSOs (i.e., CDs, CSS, and/or GPS sources) by a number of authors (Fanti et al. 1985; Fanti & Fanti 1987, 1993; Stanghellini et al. 1990, 1993; O'Dea et al. 1991) and has been simulated in some detail by De Young (1991, 1993). In the frustrated jet model, it is assumed that the ram pressure confinement due to the interstellar medium slows down the speed of advance of the jets to $\ll 0.01c$, so that these objects are much older than 10^4 yr.

It now appears most likely that CSOs are not frustrated jets, since the expansion speed is most probably comparable to that in LSOs. We therefore suggest that, apart from a small subset of MSOs in which there is good evidence of unusually strong interactions with the external medium—e.g., 3C 48 (Wilkinson et al. 1991)—the advance speeds in MSOs are comparable to those in CSOs and LSOs. Thus we believe that most MSOs are not frustrated jets but are simply young LSOs. Fanti et al. (1995) have reached a similar conclusion based on an assumed evolutionary model. We discuss this in more detail in Paper III.

Further support for this interpretation comes from the study by Heckman et al. (1994) in which they compared the mid- and far-infrared emission of GPS and CSS objects with larger radio-loud objects and found no difference. They made this study specifically to look for evidence of an unusually dense confining medium. Since they found no such evidence, they concluded that GPS and CSS could well be young.

9. GENERAL ENERGY AND LUMINOSITY CONSIDERATIONS

The bolometric radio luminosity of 2352+495 is $L_{\rm bol} = 4.8 \times 10^{43}\ h^{-2}$ ergs s^{-1}—comparable to large powerful radio galaxies and quasars. We have shown (Paper I) that any relativistic beaming in the lobes of CSOs is at most a small effect, thus the luminosity in these objects is intrinsically high. Even if the bright jet components are relativistically beamed, the bolometric luminosity has been overestimated by at most a factor 3.

The volume emissivity in these objects is $\sim 10^9$ times greater than in the largest, most luminous classical double-lobed radio sources. On the other hand, the minimum energy is 3.7×10^{54} ergs ($\sim 2\ M_\odot\ c^2$)—5 or 6 orders of magnitude less than the minimum energies of the most powerful, large radio galaxies and quasars. The combination of the bolometric radio luminosity and the minimum energy in relativistic particles and magnetic field yields a characteristic timescale, τ_c, of ~ 2500 yr. In comparison, a typical LSO (flux density 1 Jy at 5 GHz, lobe size 10, and redshift 1) has a characteristic timescale of 10^7 yr, which is comparable to the timescales derived from synchrotron aging in these objects (Alexander & Leahy 1987). Thus, the ages which we have derived for CSOs are comparable to their characteristic timescales, as is the case for the LSOs.

We have seen that the narrow line luminosity of 2352+495, after correcting for extinction, is $1.1 \times 10^{42}\ h^{-2}$ ergs s^{-1} (see Table 7). We assume that the excitation mechanism for these lines is photoionization, which suggests the presence of a continuum source of at least this luminosity in the center of activity. The Eddington limit therefore implies a mass for the central engine of $\gtrsim 10^4\ M_\odot$. We saw in § 5.1 that the total jet power in 2352+495 is $\sim 6 \times 10^{43}\ h^{-10/7}$ ergs s^{-1}, i.e., $10^{-3}\ h^{-10/7}\ M_\odot\ c^2$ per year. If we assume 10% efficiency of conversion of fuel into energetic particles and radiation, this implies an accretion rate of 0.01 $M_\odot$ per year. It is also possible that the narrow line clouds are photoionized by continuum radiation generated in shocks associated with the radio jets (Sutherland, Bicknell, & Dopita 1993).

The energy requirements of CSOs over the high-luminosity phase of activity are modest for powerful extragalactic radio sources. The bolometric radio luminosity gives an energy requirement over 10^4 yr of only 3×10^{55} ergs, i.e., $\sim 20\ M_\odot\ c^2$. Thus, assuming an efficiency of 10% in converting fuel into radio energy, a few hundred solar masses of fuel are required during the CSO phase of activity.

10. CONCLUSIONS

We have shown that Compact Symmetric Objects form a significant subset of powerful extragalactic radio sources—constituting $\sim 10\%$ of objects in high-frequency radio surveys. The bulk velocities in the jets are relativistic, but a significant fraction ($\gtrsim 33\%$) of the observed flux density in these objects is not relativistically beamed. The radio luminosity of CSOs is a larger fraction of the jet power than in most LSOs, which is likely a result of the higher external densities in CSOs.

CSOs provide a unique laboratory for the study of relativistic jets for two reasons:

1. The working surfaces in CSOs are much closer to the central engines than they are in other powerful extragalactic radio sources.
2. The advance speeds in CSOs are almost certainly sufficiently high that it should be possible to measure these directly over a decade in the most powerful CSOs at redshifts up to ~ 0.5, and in lower power CSOs at redshifts ~ 0.1. Furthermore, since the bulk motion along the jets is relativistic, it is possible to measure proper motions within the jets themselves.

The advance speed of CSOs, on our interpretation, is comparable to that of LSOs, so that ages of CSOs are $\sim 10^4$ yr. This raises interesting questions concerning the subsequent evolution of CSOs which are discussed in detail in Paper III. If CSOs evolve into typical large powerful extragalactic radio sources, then they represent a very early stage in the lifetime of objects like Cygnus A. For CSOs of sizes 3 pc–1 kpc, which can readily by studied in detail by VLBI, this covers the first 10^{-5}–3×10^{-3} of the evolutionary lifetime of classical double radio sources. If this is evolutionary sequence is correct, CSOs begin their lives at high luminosity and evolve to lower luminosities, so that the relative fraction of powerful extragalactic radio sources observed in the CSO phase is high.

In conclusion, it is now clear that the class of Compact Symmetric Objects has an important part to play in our understanding of the evolution of powerful extragalactic radio sources and of the central engines that drive them, whether these objects evolve into large-scale powerful radio sources or are a separate, short-lived, population of active galaxies.

We thank Ian Browne, Peter Goldreich, Carla and Roberto Fanti, and Peter Scheuer for their comments on an early version of this paper. We thank Chris O'Dea for making a number of useful suggestions in refereeing the

paper. We thank Diana Worrall for pointing out an error in our original determination of the X-ray limit of Figure 5. We also thank Mitch Begelman, Roger Blandford, Charles Lawrence, Phil Maloney, Nick Scoville, Sterl Phinney, and Martin Rees for helpful discussions; and we thank the staffs of the observatories in the global VLBI network and of the VLBA for their vital contributions to this work. This work was supported by grants from the National Science Foundation (AST 88-14554, AST 91-17100, and AST 94-20018). The VLBA is operated by the AUI under a grant from the National Science Foundation.

REFERENCES

Alexander, P., & Leahy, J. P. 1987, MNRAS, 225, 1
Barthel, P. D., Schilizzi, R. T., Miley, G. K., Jagers, W. J., & Strom, R. G. 1985, A&A, 148, 243
Barvainis, R., & Antonucci, R. 1994, AJ, 107, 1291
Baum, S. A., O'Dea, C. P., Murphy, D. W., & de Bruyn, A. G. 1990, A&A, 232, 19
Begelman, M. C., Blandford, R. D., & Rees, M. J. 1980, Nature, 287, 307
———. 1984, Rev. Mod. Phys., 56, 255
Blandford, R. D. 1990, in Saas-Fee Lectures: Active Galactic Nuclei, ed. R. D. Blandford, H. Netzer, & L. Woltjer (Dordrecht: Kluwer), 161
Blandford, R. D., & Rees, M. J. 1974, MNRAS, 169, 395
———. 1978, Pittsburgh Conference on BL Lac Objects, ed. A. M. Wolfe (Pittsburgh: Univ. Pittsburgh), 328
Carvalho, J. C. 1994, A&A, 292, 392
Cawthorne, T. V., Wardle, J. F. C., Roberts, D. H., Gabuzda, D. C., & Brown, L. F. 1993, ApJ, 416, 496
Conway, J. E., Myers, S. T., Pearson, T. J., Readhead, A. C. S., Unwin, S. C., & Xu, W. 1994, ApJ, 425, 568
Conway, J. E., Pearson, T. J., Readhead, A. C. S., Unwin, S. C., Xu, W., & Mutel, R. L. 1992, ApJ, 396, 62
Cutri, R. M., Huchra, J. P., Low, F. J., Brown, R. L., & Vanden Bout, P. A. 1994, ApJ, 424, L65
Dallacasa, D., Fanti, C., Fanti, R., Schilizzi, R. T., & Spencer, R. E. 1995, A&A, 295, 27
De Young, D. 1991, ApJ, 371, 69
———. 1993, ApJ, 402, 95
Efstathiou, G., Ellis, R. S., & Peterson, B. A. 1988, MNRAS, 232, 431
Ekers, R. D. 1982, Extragalactic Radio Sources, ed. D. S. Heeschen & C. M. Wade (Dordrecht: Reidel), 165
Fabbiano, G. Miller, L., Trinchieri, G., Longair, M., & Elvis, M. 1984, ApJ, 277, 115
Fanaroff, B. L., & Blake, G. M. 1972, MNRAS, 157, 41
Fanaroff, B. L., & Riley, J. M. 1974, MNRAS, 167, 31P (FR)
Fanti, C., & Fanti, R. 1987, Superluminal Radio Sources, ed. Zensus & Pearson (Cambridge: Cambridge Univ. Press), 174
———. 1993, in ASP Conf. Ser. 54 The Physics of Active Galaxies, ed. G. V. Bicknell, M. A. Dopita, & P. J. Quinn (San Francisco: ASP), 341
Fanti, C., Fanti, R., Dallacasa, D., Schilizzi, R. T., Spencer, R. E., & Stanghellini, C. 1995, A&A, 302, 317
Fanti, C., Fanti, R., Parma, P., Schilizzi, R. T., & van Breugel, W. J. M. 1985, A&A, 143, 292
Fanti, R., Fanti, C., Schilizzi, R. T., Spencer, R. E., Nan, R., Parma, P., van Breugel, W. J. M., & Venturi, T. 1990, A&A, 231, 333
Field, G. B. 1958, Proc. IRE, 46, 240
Gopal-Krishna, & Wiita, P. J. 1991, ApJ, 373, 325
Gower, A. C., Gregory, P. C., Hutchings, J. B., & Unruh, W. G. 1982, ApJ, 262, 478
Hargrave, P. J., & McEllin, M. 1975, MNRAS, 173, 37
Heckman, T. M., O'Dea, C. P., Baum, S. A., & Laurikainen, E. 1994, ApJ, 428, 65
Henstock, D., Browne, I. W. A., Wilkinson, P. N., Taylor, G. B., Vermeulen, R. C., Pearson, T. J., & Readhead, A. C. S. 1995, ApJS, 100, 1
Hunstead, R. W., Murdoch, H. S., Condon, J. J., & Phillips, M. M. 1984, MNRAS, 207, 55
Laing, R. A. 1980, MNRAS, 193, 439
Landau, L. D., & Lifshitz, E. M. 1959, in A Course of Theoretical Physics—Volume 6—Fluid Mechanics (Pergamon Press)
Lawrence, C. R., Zucker, J. R., Readhead, A. C. S., Unwin, S. C., Pearson, T. J., & Xu, W. 1996, ApJ, submitted.
Leahy, J. P. 1991, Beams & Jets in Astrophysics, ed. P. A. Hughes (Cambridge: Cambridge Univ. Press)
Lind, K. R., Payne, D. G., Meier, D. L., & Blandford, R. D. 1989, ApJ, 344, 89
Malone, P. R., Begelman, M. C., & Rees, M. J. 1994, ApJ, 432, 606
Miley, G. K. 1971, MNRAS, 152, 477
———. 1980, ARA&A, 18, 165
Mutel, R. L., Hodges, M. W., & Phillips, R. B. 1985, ApJ, 290, 86
Netzer, H. 1990, in Saas-Fee Lectures: Active Galactic Nuclei, ed. R. D. Blandford, H. Netzer, & L. Woltjer (Dordrecht: Kluwer), 57
O'Dea, C. P., Baum, S. A., & Morris, G. B. 1990, A&AS, 82, 261
O'Dea, C. P., Baum, S. A., & Stanghellini, C. 1991, ApJ, 380, 66
O'Dea, C. P., et al. 1992, in Testing the AGN paradigm, ed. S. S. Holt, S. G. Neff, & C. M. Urry (New York: AIP), 435
O'Dea, C. P., Stanghellini, C., Laurikainen, E., & Baum, S. A. 1994a, in Mass-transfer induced activity in galaxies, ed. I. Shlosman (Cambridge: Cambridge Univ. Press)
O'Dea, C. P., Worrall, D. M., Baum, S. A., & Stanghellini, C. 1995, ApJ, submitted
O'Dea, C. P., Worrall, D. M., Gilmore, D., Baum, S. A., Zirbel, E., & Stanghellini, C. 1994b, in Clusters of Galaxies: Recontre de Moriond, ed. F. Durret, A. Mazure, A. J. Tran Thanh Van (Gif-sur-Yvette: Editions Frontières), 415
Osterbrock, D. E. 1987, in Spectroscopy of Astrophysical Plasmas, ed. A. Dalgarno & D. Layzer (Cambridge: Cambridge Univ. Press), 59
———. 1989, Astrophysics of Gaseous Nebulae and Active Galactic Nuclei (Mill Valley: University Science Books)
Owen, F. N., & White, R. A. 1991, MNRAS, 249, 164
Peacock, J. A., & Wall, J. V. 1982, MNRAS, 198, 843
Pearson, T. J., Fassnacht, C., & Readhead, A. C. S. 1996, in preparation
Pearson, T. J., & Readhead, A. C. S. 1988, ApJ, 328, 114 (PR)
Perley, R. A., & Taylor, G. B. 1991, AJ, 101, 1623
Phillips, R. B., & Mutel, R. L. 1980, ApJ, 236, 89
———. 1982, A&A, 106, 21
Polatidis, A., Wilkinson, P. N., Xu, W., Readhead, A. C. S., Pearson, T. J., Taylor, G. B., & Vermeulen, R. C. 1995, ApJS, 98, 1
Rawlings, S., & Saunders, R. 1991, Nature, 349, 138
Readhead, A. C. S. 1980, Objects of High Redshift, ed. G. O. Abell & P. J. E. Peebles (Dordrecht: Reidel), 165
———. 1994, ApJ, 426, 51
Readhead, A. C. S., Cohen, M. H., Pearson, T. J., & Wilkinson, P. N. 1978, Nature, 276, 768
Readhead, A. C. S., Pearson, T. J., & Unwin, S. C. 1984, VLBI & Compact Radio Sources, ed. R. Fanti, K. Kellermann, & G. Setti (Dordrecht: Reidel), 131
Readhead, A. C. S., Taylor, G. B., Pearson, T. J., & Wilkinson, P. N. 1996, ApJ, in press (Paper III)
Rudnick, L., & Jones, T. W. 1983, AJ, 88, 518
Sanders, D. B., Scoville, N. Z., & Soifer, B. T. 1991, ApJ, 370, 158
Scheuer, P. A. G. 1974, MNRAS, 166, 513
———. 1982, in IAU Symp. 97, Extragalactic Radio Sources, ed. D. S. Heeschen & C. M. Wade (Dordrecht: Reidel), 163
Schinke, R., Engel, V., Buck, U., Mayer, H., & Diercksen, G. H. F. 1985, ApJ, 299, 939
Scoville, N. Z. 1994, in The Nuclei of Normal Galaxies, ed. R. Genzel & A. T. Harris (Dordrecht: Kluwer), 117
Scoville, N. Z., Sargent, A. I., Sanders, D. B., & Soifer, B. T. 1989, ApJ, 366, L5
Shepherd, M. C., Pearson, T. J., & Taylor, G. B. 1994, BAAS, 26, 987
Shostak, G. S., van Gorkom, J. H., Ekers, R. D., Sanders, R. H., Goss, W. M., & Cornwell, T. J. 1983, A&A, 119, L3
Soifer, B. T., et al. 1984, ApJ, 283, L1
Stanghellini, C., Baum, S. A., O'Dea, C. P., & Morris, G. B. 1990, A&A, 233, 379
Stanghellini, C., O'Dea, C. P., Baum, S. A., & Laurikainen, E. 1993, ApJS, 88, 1
Sutherland, R. S., Bicknell, G. V., & Dopita, M. A. 1993, ApJ, 414, 510
Taylor, G. B., & Perley, R. A. 1993, ApJ, 416, 544
Taylor, G. B., Readhead, A. C. S., & Pearson, T. J. 1996, ApJ, in press
Taylor, G. B., Vermeulen, R. C., & Pearson, T. J. 1995, Proc. Natl. Acad. Sci., 92, 11381
Taylor, G. B., Vermeulen, R. C., Pearson, T. J., Readhead, A. C. S., Henstock, D., Browne, I. W. A., & Wilkinson, P. N. 1994, ApJS, 95, 345
Thakkar, D. D., Xu, W., Readhead, A. C. S., Pearson, T. J., Taylor, G. B., Vermeulen, R. C., Wilkinson, P. N., & Polatidis, A. 1995, ApJS, 98, 33
van Breugel, W. 1984, VLBI & Compact Radio Sources, ed. R. Fanti, K. Kellermann, & G. Seti (Dordrecht: Reidel), 59
van der Hulst, J. M., Golisch, W. F., & Haschick, A. D. 1983, ApJ, 264, L37
van Gorkom, J. H., Knapp, G. R., Ekers, R. D., Ekers, D. D., Laing, R. A., & Polk, K. S. 1989, A&A, 97, 708
———. 1990, in Dynamics and Interactions of Galaxies, ed. R. Wielen (Berlin: Springer), 308
Wilkinson, P. N., Polatidis, A., Readhead, A. C. S., Xu, W., & Pearson, T. J. 1994, ApJ, 432, L87 (Paper I)
Wilkinson, P. N., Polatidis, A., Xu, W., Readhead, A. C. S., & Pearson, T. J. 1993, Subarcsecond Radio Astronomy, ed. R. J. Davis & R. S. Booth (Cambridge: Cambridge Univ. Press), 213

Wilkinson, P. N., Tzioumis, A. K., Benson, J. M., Walker, R. C., Simon, R. S., & Kahn, F. D. 1991, Nature, 352, 313
Xu, W. 1994, Ph.D. thesis, California Institute of Technology.
Xu, W., Pearson, T. J., Taylor, G. B., Readhead, A. C. S., Wilkinson, P. N., & Polatidis, A. 1995, ApJS, in press
Zensus, J. A., & Pearson, T. J. 1987, Superluminal Radio Sources (Cambridge: Cambridge Univ. Press)
———. 1990, Parsec-scale Radio Jets (Cambridge: Cambridge Univ. Press)